

Many-body quantum dynamics of an asymmetric bosonic Josephson junction

Sudip Kumar Haldar^{1,2} and Ofir E. Alon^{1,2}

¹*Department of Mathematics, University of Haifa, Haifa 3498838, Israel.*

²*Haifa Research Center for Theoretical Physics and Astrophysics,
University of Haifa, Haifa 3498838, Israel.*

(Dated: November 9, 2021)

Abstract

The out-of-equilibrium quantum dynamics of an interacting Bose gas trapped in a one-dimensional asymmetric double-well potential is studied by solving the many-body Schrödinger equation numerically accurately. We examine how the loss of symmetry of the confining trap affects the macroscopic quantum tunneling dynamics of the system between the two wells. In an asymmetric double well, the two wells are not equivalent anymore - the left well is deeper than the right one. Accordingly, we analyze the dynamics by initially preparing the condensate in both the left and the right well. The dynamics of the system is characterized by the time evolution of a few physical quantities of increasing many-body complexity, namely, the survival probability, depletion and fragmentation, and the many-particle position and momentum variances. In particular, we have examined the frequencies and amplitudes of the oscillations of the survival probabilities, the time scale for the development of fragmentation and its degree, and the growth and oscillatory behavior of the many-particle position and momentum variances. There is an overall suppression of the oscillations of the survival probabilities in an asymmetric double well. However, depending on whether the condensate is initially prepared in the left or right well, the repulsive inter-atomic interactions affect the survival probabilities differently. For a sufficiently strong repulsive interaction, the system is found to become fragmented. The degree of fragmentation depends both on the asymmetry of the trap and the initial well in which the condensate is prepared in a non-trivial manner. Overall, the many-particle position and momentum variances bear the prominent signatures of the density oscillations of the system in the asymmetric double well as well as a breathing-mode oscillation. Finally, a universality of fragmentation for systems made of different numbers of particles but the same interaction parameter is also found. The phenomenon is robust despite the asymmetry of the junction and admits a macroscopically-large fragmented condensate characterized by a diverging many-particle position variance. This is as far as one can get from the dynamics of the density in the junction.

PACS numbers: 03.75.Lm,05.60.Gg,05.30.Jp,67.85.-d

I. INTRODUCTION

The dynamics of ultra-cold quantum gases has attracted a lot of interest since the experimental observations of Bose-Einstein condensation (BEC) [1–3]. The advent of advanced trapping techniques and controlling of inter-particle interactions has made it possible to experimentally study several problems which were elusive until recently. This has opened a whole new research field of strongly correlated systems with potential applications in various fields such as quantum computing and quantum simulation of condensed-matter problems [4–7]. One such well-studied example is the system of a few interacting bosons in a double-well potential [8–25].

A symmetric double-well potential provides a paradigm model for many physical systems such as the bosonic Josephson junction (BJJ) [26]. BJJ dynamics has been studied quite thoroughly both theoretically and experimentally [8–12, 18, 21, 26–45]. Several features like Josephson oscillations [8, 9, 18, 21, 29, 39–41], collapse and revival cycles [10], self trapping (suppression of tunneling) [8–10, 21, 29, 39], etc. have been predicted using a two-mode theory and later experimentally observed [9]. Recently, BJJ dynamics has also been studied by an in-principle numerically-exact many-body theory [42–44]. In particular, fragmentation [44, 46] and the uncertainty product of the many-particle position and momentum operators [47] have been studied by solving the many-body Schrödinger equation. Further, a universality of fragmentation in the sense that systems with different particle numbers N , keeping the interaction parameter $\Lambda = \lambda_0(N-1)$ fixed (λ_0 being the strength of interaction), fragment to the same value [44] has been predicted in the dynamics of interacting bosons in a symmetric double well for a sufficiently strong interaction. Also, the impact of the range of the interaction on the dynamics of a BJJ has been investigated recently [45].

Symmetry breaking is of fundamental interest in physics. Accordingly, an asymmetric double well is of particular interest. Already a number of studies of the properties of an ultra-cold atomic system in an asymmetric double well trap and a few of its applications have been reported [48–56]. For example, a novel sensor utilizing the adiabatic axial splitting of a BEC in an asymmetric double well has been reported [48]. The ground state properties of spin-1 bosons [52] in an asymmetric double well has also been studied. Also, the ground state properties and the corresponding transition between the Josephson and self-trapped regimes for an attractive BEC have been studied by the two-site Bose-Hubbard model [49].

Moreover, the tunneling of a two-boson system [50] and the interaction blockade for a few boson-system with up to $N = 3$ bosons [56] in an asymmetric double well have also been studied. A two-mode model has been constructed to study the dynamics of a BEC in an asymmetric double well and its phase-space properties are analyzed [51]. However, a systematic study of the dynamics of a many-particle bosonic system in an asymmetric double well for different interaction regimes using a numerically-exact many-body method is, to the best of our knowledge, yet to be reported. Such a method automatically includes all participating bands in the asymmetric double well. This allows us to describe the physics of the asymmetric BJJ both when it is fully condensed and when it becomes fragmented on an accurate many-body level.

Therefore in this work, we ask how the loss of symmetry in the double well trap may affect the many-body physics of BJJ dynamics for different strengths of interaction. Since BJJ dynamics involves macroscopic quantum tunneling, such studies are of general interest. Here we consider a short-range contact δ interaction of tunable strength λ_0 which is the popular model for inter-atomic interaction in ultra-cold atomic systems [57]. In this work, we examine the impact of different degrees of asymmetries, for different strengths of interactions, on the dynamics of BEC in an asymmetric double well following a trapping quench from a single harmonic well to the asymmetric double well at time $t = 0$. Moreover, in an asymmetric double well, the two wells are not equivalent anymore and for the kinds of asymmetric double wells considered in this work, the left well is lower than the right well. Accordingly, we study the non-equilibrium dynamics of the system following the trapping quench by preparing the BEC in the left and the right wells, and ascertain how the dynamics depends on the initial well.

For our study, we numerically accurately solve the many-body Schrödinger equation [46] and characterize the dynamics of the system by the time evolution of a few physical quantities of varying degrees of complexity, both at the mean-field and the many-body level. We focus on the time evolution of the survival probability, depletion and fragmentation, and the variance of the many-particle position and momentum operators. We examine both the weakly-interacting system as well as that with a stronger interaction where the system becomes fragmented, and thereby explore how the many-body features develop in these quantities in different interaction regime. Therefore, in this work, our scope of investigation is far beyond that of Ref [44] where only the strong interaction case was considered.

More importantly for the first time, the time evolution of the many-particle position and momentum variances in the junction are discussed in this work.

The density oscillations of a BEC is found to be suppressed in an asymmetric double well. However, the repulsive inter-atomic interaction facilitates the tunneling between the two wells when the initial condensate is prepared in the left well. On the other hand, if the initial BEC is prepared in the right well, the repulsive interaction suppresses the oscillations further. For a stronger interaction, the BEC becomes fragmented and the degree of fragmentation is found to depend on the initial well. Further, a universality of the fragmentation dynamics is also observed, though again the degree of the universal fragmentation differs for the left and the right well. We also found prominent signatures of density oscillations as well as breathing-mode oscillations in the time evolution of the variances of the many-particle position and momentum operators. Note that for the description of the breathing mode oscillations, one needs to take into account the coupling with higher energy bands and, therefore, it is beyond the scope of Bose-Hubbard dimer.

This paper is organized as follows. In Section II, we introduce the quantities which will be used to characterize the dynamics and also the in principle numerically-exact many-body method used to solve the time-dependent many-body Schrödinger equation. In Section III, we present and discuss our findings. Finally, we summarize and put our concluding remarks in Section IV. Numerical convergence is discussed in the Appendix.

II. THEORETICAL FRAMEWORK

In this section, we introduce the theoretical methods and quantities used in this work to explore the dynamics of an asymmetric bosonic Josephson junction.

A. System

Here we are interested in the dynamics of a system of N interacting structureless bosons in a one-dimensional (1D) asymmetric double well which is governed by the time-dependent

many-body Schrödinger equation:

$$\hat{H}\Psi = i\frac{\partial\Psi}{\partial t},$$

$$\hat{H}(x_1, x_2, \dots, x_N) = \sum_{j=1}^N \hat{h}(x_j) + \sum_{k>j=1}^N W(x_j - x_k). \quad (1)$$

Here x_j is the coordinate of the j -th boson, $\hat{h}(x) = \hat{T}(x) + V_T(x)$ is the one-body Hamiltonian containing kinetic energy and trapping potential $V_T(x)$ terms, and $W(x_j - x_k)$ is the pairwise interaction between the j -th and k -th bosons. Dimensionless units are employed throughout this work. The asymmetric double well $V_T(x)$ is constructed by adding a linear slope of gradient C to the symmetric double well which itself is obtained by fusing two slightly shifted harmonic potential $V_{L,R} = \frac{1}{2}(x \pm 2)^2 + Cx$, i.e.,

$$V_T(x) = \begin{cases} \frac{1}{2}(x+2)^2 + Cx, & x < -\frac{1}{2} \\ \frac{3}{2}(1-x^2) + Cx, & |x| \leq \frac{1}{2} \\ \frac{1}{2}(x-2)^2 + Cx, & x > \frac{1}{2} \end{cases}. \quad (2)$$

The symmetric double-well part is taken from [45]. This will allow us to relate and compare results in the asymmetric junctions to that in the symmetric one. The shape of an asymmetric double well for $C = 0.01$ used in this work along with its first few energy levels E_n and eigenstates $\varphi_n(x)$ are shown in Fig. 1(a). One can see that it is hardly distinguishable from the symmetric double well. Also, even for such a small asymmetry C , the superposition of the first two eigenstates are not completely localized in one or the other well, thereby affecting the density oscillations between the two wells. Moreover, the spacing between the two successive energy levels increases as one goes up the spectrum: while the lowest two energy levels lie very close to each other and form the lowest energy band, the higher energy levels from E_5 onward are practically unaffected by the barrier between the two wells and form an almost uniform spectrum. Therefore, the dynamics of the system in such an asymmetric double well is primarily controlled by the lowest energy band. However, with increasing C , the spectrum starts to be affected more prominently by the asymmetry and the higher energy levels begin to play more important role in the dynamics.

To highlight the point further, we compute the ratio of the inter-band spacing to the intra-band spacing of the lowest band, viz., $\frac{\Delta E_{n2}}{\Delta E_{21}} = \frac{E_n - E_2}{E_2 - E_1}$. In Fig. 1(b), we explicitly show the ratios $\frac{\Delta E_{32}}{\Delta E_{21}}$ and $\frac{\Delta E_{52}}{\Delta E_{21}}$ as functions of C . We see that starting from a relatively large

value for the symmetric double well ($C = 0$), these ratios decay rapidly with C with the decay rate being higher for $\frac{\Delta E_{52}}{\Delta E_{21}}$. This implies that coupling to higher energy levels starts to grow with increasing C . For the range of values of C of our interest [shown in the inset of Fig. 1(b)], we see that the $\frac{\Delta E_{32}}{\Delta E_{21}}$ and $\frac{\Delta E_{52}}{\Delta E_{21}}$ are quite large and of the order of their values for the $C = 0$. Therefore, in the regime of our interest, the lowest energy band is expected to play the lead role in the dynamics of the system. However, the next nearest band may influence the dynamics by giving rise to the breathing mode oscillations on top of the Rabi oscillations controlled primarily by the lowest band. Also, in our present study, the inter-atomic interaction $W(x_j - x_k)$ may lead to a coupling with the higher energy levels. Therefore, even for such a small asymmetry, it is necessary to effectively take all bands into account. Only then, one can be sure that the lowest band is the dominant one.

The time period of the Rabi oscillations in the double well, $t_{Rabi} = \frac{2\pi}{E_2 - E_1}$, provides a natural choice for the time scale of the dynamics. t_{Rabi} as a function of the asymmetry C is shown in Fig. 1(c) with the region of our interest being highlighted in the inset. We note that t_{Rabi} also decreases exponentially with C . Actually, for a small asymmetry C , the ground state and the first excited state in the asymmetric double well are delocalized, and t_{Rabi} gives the time period of Rabi oscillations in the double well. However, for large C , the barrier becomes very high and there is no tunneling back and forth between the two wells. Then E_1 and E_2 become the lowest two energy levels in the lower well $V_L(x)$ and $\frac{2\pi}{E_2 - E_1}$ is associated with the time period of breathing mode oscillations. In this work, as already mentioned above, we consider only small asymmetries and therefore, we will use the time period of Rabi oscillations t_{Rabi} as a unit of time for the description of the dynamics in a particular asymmetric double well trap. However, as shown above, t_{Rabi} varies with C and therefore is not suitable for comparing the dynamics in different asymmetric traps. However, from the inset of Fig 1(c), we note that for the range of values of C of our interest $t_{Rabi} \sim 10^{-2}$ and, therefore, for comparing the dynamics in different traps, we will use $t_0 = 100$ as a unit of time.

Further, it is convenient to define the different quantities of interest in terms of the one-body and the two-body reduced density matrices [58–61] instead of the full many-body wavefunction. Given the normalized many-body wavefunction $\Psi(t)$, the reduced one-body

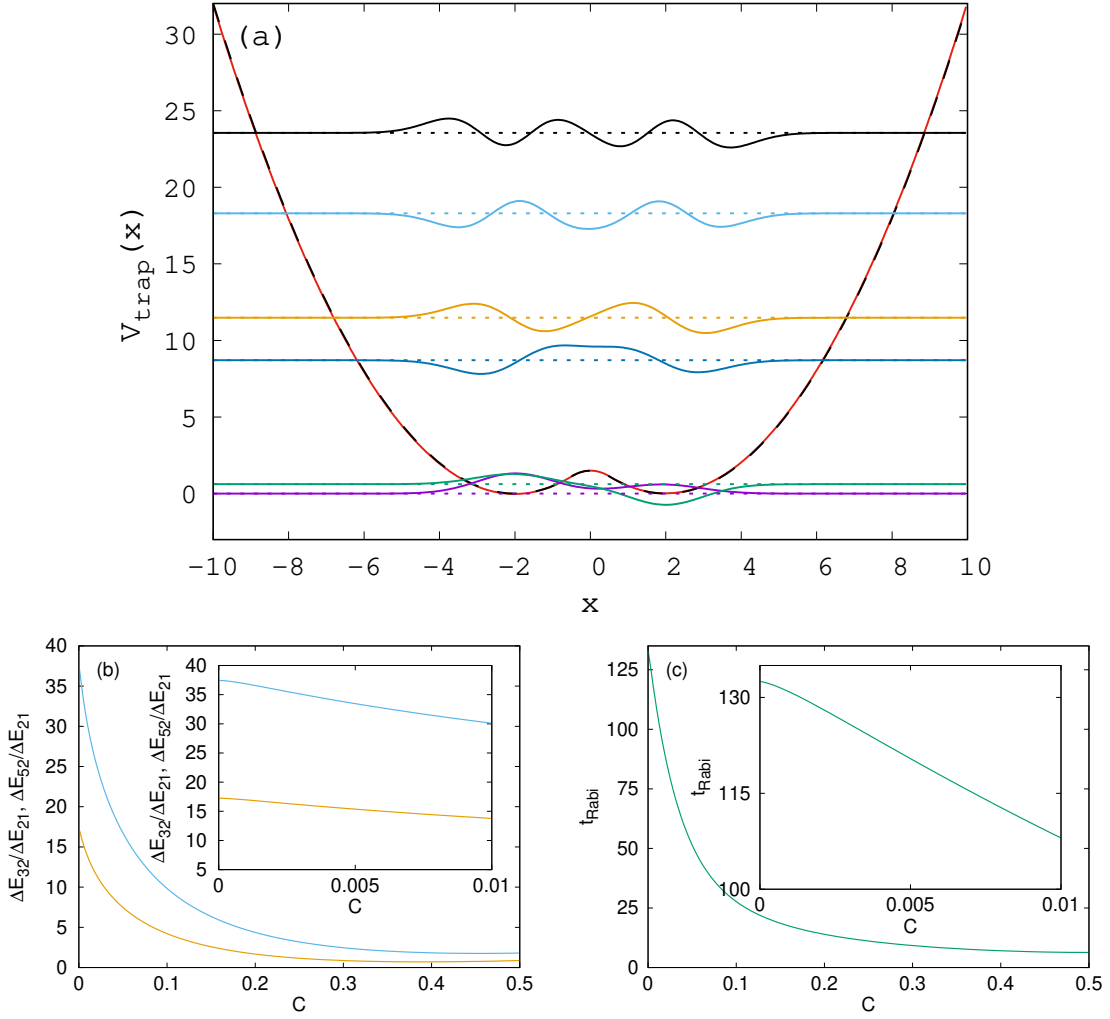


FIG. 1. (a) An asymmetric double well potential with a small asymmetry $C = 0.01$ (red solid curve) and its first six eigenfunctions. The symmetric double well (yellow dashed curve) is also shown for comparison. A ten times magnified view of the relative positions of the energy levels with respect to the ground state is presented as the dotted horizontal lines while the horizontal solid curves represent a ten times magnified view of the corresponding eigenstates. The color code used for presenting the energy levels and the eigenstates is as follows: Magenta corresponds to the ground state, green to the first excited state, dark blue for the second excited state, dark yellow the third, sky blue the fourth and black presents the fifth excited state. (b) Ratio of the inter-band spacing to the intra-band spacing of the lowest band as a function of the asymmetry C for the first and second higher band. The yellow curve represents $\frac{\Delta E_{52}}{\Delta E_{21}}$ while the sky blue curve represents the $\frac{\Delta E_{32}}{\Delta E_{21}}$. (c) t_{Rabi} as a function of C . In the inset of panel (b) and (c), the range of C considered in this work is highlighted. See text for details. The quantities shown are dimensionless.

density matrix can be calculated as

$$\begin{aligned}\rho^{(1)}(x_1|x'_1; t) &= N \int dx_2 \dots dx_N \Psi^*(x'_1, x_2, \dots, x_N; t) \\ &\quad \times \Psi(x_1, x_2, \dots, x_N; t) \\ &= \sum_{j=1}^M n_j(t) \phi_j^{*NO}(x'_1, t) \phi_j^{NO}(x_1, t).\end{aligned}\tag{3}$$

Here, $\phi_j^{NO}(x_1, t)$ are the time-dependent natural orbitals and $n_j(t)$ the time-dependent natural occupation numbers. The natural occupations $n_j(t)$ are used to characterize the (time varying) degree of condensation in a system of interacting bosons [62] and satisfy $\sum_{j=1}^M n_j = N$ (M is the number of single particle orbitals used to construct the many-boson wavefunction, see Sec. IIC). If only one macroscopic eigenvalue $n_1(t) \approx \mathcal{O}(N)$ exists, the system is condensed [62] whereas if there are more than one macroscopic eigenvalues, the BEC is said to be fragmented [46, 61, 63–66]. The diagonal of the $\rho^{(1)}(x_1|x'_1; t)$ gives the density of the system $\rho(x; t) \equiv \rho^{(1)}(x|x' = x; t)$.

Similarly, the two-body density can be calculated as

$$\begin{aligned}\rho^{(2)}(x_1, x_2|x'_1, x'_2; t) &= \\ N(N-1) \int dx_3 \dots dx_N \Psi^*(x'_1, x'_2, x_3, \dots, x_N; t) \\ &\quad \times \Psi(x_1, x_2, x_3, \dots, x_N; t).\end{aligned}\tag{4}$$

Therefore, the matrix elements of the two-body reduced density matrix are given by $\rho_{ksql} = \langle \Psi | b_k^\dagger b_s^\dagger b_q b_l | \Psi \rangle$ where b_k and b_k^\dagger are the bosonic annihilation and creation operators, respectively.

B. Physical quantities

In this work, we will study the dynamics of the system by exploring the time evolution of different physical quantities defined as follows. While some of these quantities can be studied both at the mean-field and the many-body levels, others can only be studied at the many-body level.

- a) *Survival probability.* In the dynamics of BEC in an asymmetric double well following a trapping quench from a harmonic well to an asymmetric double well at $t = 0$, we can prepare the initial BEC state either in the left well (L) or in the right well (R).

Accordingly, we can calculate two types of survival probabilities. For starting with the initial BEC state in the left well, we can define the survival probability in the left well $[p_L(t)]$ as

$$p_L(t) = \int_{-\infty}^0 dx \frac{\rho_L(x;t)}{N}, \quad (5)$$

where $\rho_L(x;t)$ is the density when the initial BEC state is prepared in the left well. Similarly, when the initial state is prepared in the right well, the survival probability in the right well $[p_R(t)]$ can be defined as

$$p_R(t) = \int_0^{\infty} dx \frac{\rho_R(x;t)}{N}, \quad (6)$$

where $\rho_R(x;t)$ is the density when the initial condensate is in the right well. For a symmetric double well, both $\rho_R(t)$ and $\rho_L(t)$ are equivalent and therefore we have only a single type of survival probability $p(t)$, i.e., $p_L(t) \equiv p_R(t) = p(t)$. Since the density can be studied both at the mean-field and the many-body levels, survival probabilities can also be calculated both at the mean-field and the many-body levels.

b) *Depletion and fragmentation.* As discussed above, when $n_1(t) \approx \mathcal{O}(N)$ the system is condensed and the sum over all the microscopic fractions of occupations in the higher orbitals $f = \sum_{j=2}^M \frac{n_j}{N}$ (M is the number of orbital, see above) is known as the depletion per particle. On the other hand for a fragmented system, the macroscopic occupation of a higher natural orbital, viz. $f = \frac{n_{j>1}}{N}$ where $n_j \approx \mathcal{O}(N)$, is called fragmentation. From the definition, it is clear that one needs more than one orbital to study the depletion and fragmentation and hence, these quantities can only be calculated by at least a two-orbital many-body theory and preferably a multi-orbital many-body theory. We remark that the depletion of a BEC is usually small and may not have a prominent effect on the density per particle and energy per particle which, in effect, can be accurately described by a mean-field theory. However, fragmentation can have a dominant effect on the energy per particle and the density per particle of the system. Moreover, though the depletion and the fragmentation are physically different quantities and appear under different conditions, for a two-orbital theory they have the same mathematical expression. Accordingly, for the computation with $M = 2$ orbitals only we will refer to both of them by f , see Sec. II C below.

c) *many-particle position and momentum variance.* The quantum variance of an observ-

able is a fundamental quantity in quantum mechanics due to its connection with the uncertainty principle. It gives a measure of the quantum resolution with which an observable can be measured. For any many-body operator $\hat{A} = \sum_{j=1}^N \hat{a}(x_j)$ where $\hat{a}(x_j)$ is a Hermitian operator and local in position space, the variance per particle $\frac{1}{N}\Delta_{\hat{A}}^2(t)$ [47, 67–69] is given by

$$\begin{aligned} \frac{1}{N}\Delta_{\hat{A}}^2(t) &= \frac{1}{N} \left[\langle \Psi(t) | \hat{A}^2 | \Psi(t) \rangle - \langle \Psi(t) | \hat{A} | \Psi(t) \rangle^2 \right] \equiv \Delta_{\hat{a},density}^2(t) + \Delta_{\hat{a},MB}^2(t), \\ \Delta_{\hat{a},density}^2(t) &= \int dx \frac{\rho(x;t)}{N} a^2(x) - \left[\int dx \frac{\rho(x;t)}{N} a(x) \right]^2, \\ \Delta_{\hat{a},MB}^2(t) &= \frac{\rho_{1111}(t)}{N} \left[\int dx |\phi_1^{NO}(x;t)|^2 a(x) \right]^2 - (N-1) \left[\int dx \frac{\rho(x;t)}{N} a(x) \right]^2 + \\ &\sum_{jpkq \neq 1111} \frac{\rho_{jpkq}(t)}{N} \left[\int dx \phi_j^{*NO}(x;t) \phi_k^{NO}(x;t) a(x) \right] \left[\int dx \phi_p^{*NO}(x;t) \phi_q^{NO}(x;t) a(x) \right]. \end{aligned} \quad (7)$$

Here the first term, $\Delta_{\hat{a},density}^2(t)$, is the variance of $\hat{a}(x)$ resulting from the density per particle $\frac{\rho(x;t)}{N}$, whereas the second term, $\Delta_{\hat{a},MB}^2(t)$, takes into account all other contributions to the many-particle variance. Similar expressions hold for operators which are local in momentum space. We point out that one can, in principle, study the variance of any operator at the mean-field level by substituting the many-body wavefunction $\Psi(t)$ by the corresponding mean-field wavefunction. However, in the mean-field theory, only $\Delta_{\hat{a},density}^2(t)$ has a nonzero contribution while $\Delta_{\hat{a},MB}^2(t)$ is identically equal to zero. Therefore, even for the interaction strengths for which the mean-field theory is expected to accurately describe the density per particle of the system, the many-body variance can deviate from its mean-field result. Accordingly, in this work we will consider the variances of the many-particle position and momentum operators at the many-body level only.

C. Computational Method

The time-dependent many-boson Schrödinger equation (1) cannot be solved exactly (analytically), except for a few specific cases only, see, e.g., [70]. Hence, to solve Eq. (1) in-principle numerically exactly, the multi-configurational time-dependent Hartree method for bosons (MCTDHB), [71, 72] was developed and benchmarked with an exactly-solvable model [73, 74]. This method has already been extensively used in the literature [42, 45,

56, 75–82]. Detailed derivation of the MCTDHB equation of motions can be found in [72]. Below we briefly describe the basic idea behind the method.

In MCTDHB, the ansatz for solving Eq. (1) is obtained by the superposition of all possible $\binom{N+M-1}{N}$ configurations, obtained by distributing N bosons in M time-dependent single-particle states $\phi_k(x, t)$, which we call orbitals, i.e.,

$$|\Psi(t)\rangle = \sum_{\vec{n}} C_{\vec{n}}(t) |\vec{n}; t\rangle, \quad (8)$$

where the occupations $\vec{n} = (n_1, n_2, \dots, n_M)$ preserve the total number of bosons N . For an exact theory, M should be infinitely large. However, for numerical computations one has to truncate the series at a finite M . In actual calculations, we keep on increasing M until we reach the convergence with respect to M and thereby we obtain a numerically-exact result. In the context of bosons in a double-well, the latter implies that the MCTDHB theory effectively takes all required bands into account. Here we would like to point out that for $M = 1$, the ansatz Eq. (8) gives back the ansatz for the Gross Pitaevskii theory [57].

Therefore, solving for the time-dependent wavefunction $\Psi(t)$ boils down to the determination of the time-dependent coefficients $\{C_{\vec{n}}(t)\}$ and the time-dependent orbitals $\{\phi_k(x, t)\}$. Employing the usual Lagrangian formulation of the time-dependent variational principle [83, 84] subject to the orthonormality between the orbitals, the working equations of the MCTDHB are obtained as follows

$$\begin{aligned} i \left| \dot{\phi}_j \right\rangle &= \hat{\mathbf{P}} \left[\hat{h} |\phi_j\rangle + \sum_{k,s,q,l=1}^M \{\boldsymbol{\rho}(t)\}_{jk}^{-1} \rho_{ksql} \hat{W}_{sl} |\phi_q\rangle \right]; \\ \hat{\mathbf{P}} &= 1 - \sum_{j'=1}^M |\phi_{j'}\rangle \langle \phi_{j'}| \\ \mathbf{H}(t)\mathbf{C}(t) &= i \frac{\partial \mathbf{C}(t)}{\partial t}. \end{aligned} \quad (9)$$

Here, $\boldsymbol{\rho}(t)$ is the reduced one-body density matrix [Eq. (3)], ρ_{ksql} are the elements of the two-body reduced density matrix [Eq. (4)], and $\mathbf{H}(t)$ is the Hamiltonian matrix with the elements $H_{\vec{n}\vec{n}'}(t) = \langle \vec{n}; t | \hat{H} | \vec{n}'; t \rangle$. A parallel version of MCTDHB has been implemented using a novel mapping technique [85, 86]. We mention that by propagating in imaginary time the MCTDHB equations also allow one to determine the ground state of interacting many-boson systems, see [46, 73]. In our present work we have performed all computations

with $M = 2$ time-adaptive orbitals. By repeating our computations with $M = 4, 6$, and 8 orbitals the results have been verified and found to be highly accurate for the quantities and propagation times considered here. Further details about our numerical computations and its convergence are discussed in the Appendix.

III. RESULTS

In this section, we discuss the outcome of our investigation of the dynamics of a BEC in an asymmetric double well. Specifically, we are interested to understand how the presence of asymmetry influences the overall dynamics of the BEC for different interaction strengths. In this work, we consider the dynamics of systems made of $N = 100 - 10000$ bosons interacting via a contact δ interaction of strength λ_0 which corresponds to the interaction parameter $\Lambda = \lambda_0(N - 1)$. We again remind that for an asymmetric double well trap, one can prepare the initial state either in the left well $V_L(x)$ or in the right well $V_R(x)$, and then allow the system to evolve in time in the double well $V_T(x)$. Accordingly, we will study the dynamics of the system once starting from $V_L(x)$ and then from $V_R(x)$.

A. Quantum dynamics in an asymmetric double-well

As already mentioned above, we will characterize the dynamics in an asymmetric double well trap by the time evolution of a few physical quantities such as the survival probability, depletion and fragmentation, and the many-particle position and momentum variances. The corresponding dynamics in the symmetric double well will serve as a reference for our analysis. We studied the time evolution of these quantities at the many-body levels for a weak as well as a strong interaction strength Λ . We also studied the corresponding dynamics at the mean-field level, wherever applicable, to explicitly highlight the many-body effects in the dynamics.

1. Survival probability

We start with the survival probability $p(t)$ in the initial well (left well) of a symmetric double well which will serve as the reference for our subsequent analysis of the survival

probabilities $p_L(t)$ and $p_R(t)$ in an asymmetric double well. As discussed above, the survival probabilities can be studied both at the mean-field and many-body levels. Accordingly, in Fig. 2(a) we plot the mean-field results of $p(t)$ for different Λ . We see that $p(t)$ performs smooth oscillations back and forth between the two wells. For a symmetric double well, the one-body Hamiltonian $\hat{h}(x)$ is invariant under parity and therefore its eigenstates are also parity eigenstates: the ground state has even parity while the first excited state is odd. Accordingly, the superpositions of these two states are localized in one or the other well. Therefore, when a one-particle state initially localized in one well is allowed to evolve in time, it keeps on tunneling back and forth between the two wells. However, in case of systems with a finite number of interacting particles like a BEC, there will be an effect of inter-particle interactions on this tunneling dynamics. Such effects are manifested through the frequency of oscillations of $p(t)$ in Fig. 2(a). We observe that, as the inter-atomic interaction Λ increases, the frequency of oscillations of $p(t)$ decreases. In the same figure, we also plot the many-body results of $p(t)$ for $N = 1000$, $\Lambda = 0.01$, and $M = 2$ orbitals. The complete overlap between the mean-field and the many-body results of $p(t)$ confirms that for these parameters, the density per particle of the system and hence the survival probability can be accurately described by the mean-field theory.

Next, we consider an asymmetric double well potential with a very small asymmetry, $C = 0.001$. Due to the presence of asymmetry, the parity symmetry of $\hat{h}(x)$ is now lifted and therefore, the eigenstates of $\hat{h}(x)$ are no more parity eigenstates. Accordingly, the superpositions of the first two eigenstates of $\hat{h}(x)$ (see Fig. 1) are no longer well localized in one or the other well. Therefore, if a one-particle state initially localized in one well is allowed to evolve in time, it will become partially delocalized over both wells and hence there will never be full oscillations of the density of the system between the two wells.

However, for such a small asymmetry $C = 0.001$ and a weak interaction $\Lambda = 0.01$, we did not find any visible suppression of oscillations of $p_L(t)$ and $p_R(t)$ at the mean-field level (not shown here). Moreover, both $p_L(t)$ and $p_R(t)$ would lie on top of each other. Therefore, we conclude that $C = 0.001$ is too small of an asymmetry to have any visible impact on the tunneling dynamics of the system. We also repeat our calculations of $p_L(t)$ and $p_R(t)$ for a system of $N = 1000$ interacting bosons by the MCTDHB method with $M = 2$ orbitals and confirm that these mean-field descriptions of $p_L(t)$ and $p_R(t)$ are accurate.

Next, we enhance the asymmetry to $C = 0.01$ keeping $\Lambda = 0.01$ fixed. The mean-

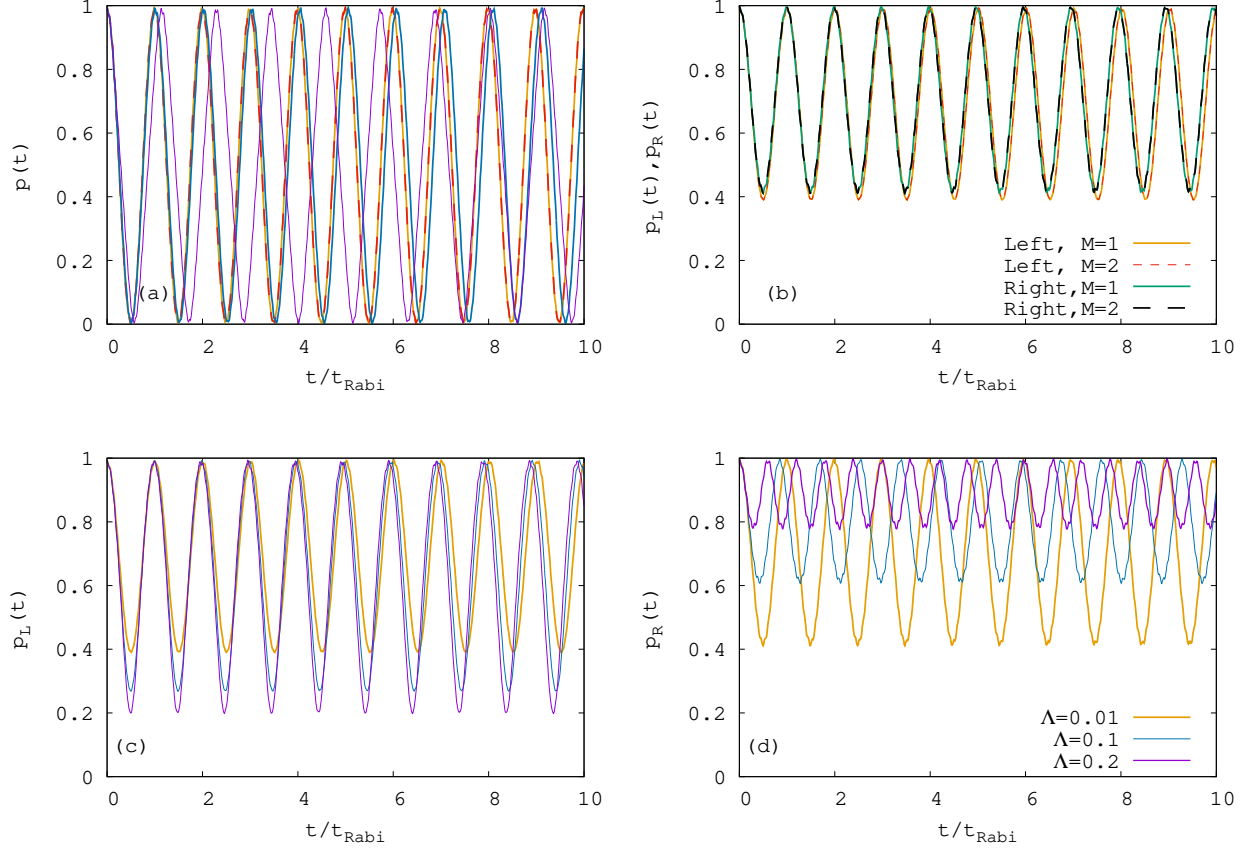


FIG. 2. (a) Time evolution of the survival probability $p(t)$ in the left well of a symmetric double well for different interaction strengths Λ . Mean-field results of $p(t)$ for $\Lambda = 0.01$ (largest amplitude), $\Lambda = 0.1$ (intermediate amplitude), and $\Lambda = 0.2$ (smallest amplitude) correspond to the yellow, blue, and magenta smooth curves, respectively. The MCTDHB result of $p(t)$ computed with $M = 2$ orbitals for a system of $N = 1000$ bosons and $\Lambda = 0.01$ is shown as the red dashed curve. (b) Time evolution of the survival probabilities in the left [$p_L(t)$] and right [$p_R(t)$] well of an asymmetric double well with asymmetry $C = 0.01$ for $\Lambda = 0.01$. The yellow smooth curve corresponds to the mean-field result of $p_L(t)$ while the red dashed curve represents the MCTDHB result of $p_L(t)$ computed with $M = 2$ orbitals for a system of $N = 1000$ bosons. On the other hand, the green smooth curve represents the corresponding mean-field result of $p_R(t)$ while the corresponding MCTDHB result computed with $M = 2$ orbitals for a system of $N = 1000$ bosons is shown as the black dashed curve. (c) Mean-field results of the time evolution of the survival probability in the left [$p_L(t)$] well of an asymmetric double well with asymmetry $C = 0.01$ for different Λ . Color codes are explained in panel (d). (d) The corresponding mean-field time evolution of the the survival probability in the right well [$p_R(t)$]. The quantities shown here are dimensionless.

field $p_L(t)$ and $p_R(t)$ are shown in Fig. 2(b). Now, we observe the expected suppression of tunneling between the two wells. The amplitudes of oscillations of both p_L and p_R have decreased by nearly 40% indicating that almost 40% of the system does not tunnel out of the initial well. Moreover, though $p_L(t)$ and $p_R(t)$ practically overlap with each other, a small phase difference is found to develop with time after a few oscillations. This small phase difference is the combined effect of asymmetry and such weak interaction on the dynamics. In the same figure, we also plot the many-body $p_L(t)$ and $p_R(t)$ obtained with $M = 2$ orbitals. That the respective mean-field and many-body curves for $p_L(t)$ and $p_R(t)$ again lie atop each other confirms that the mean-field description of the system is accurate for such a weak Λ . Thus, here we observe that even an asymmetry as small as $C = 0.01$ has a prominent effect on the macroscopic tunneling dynamics of the system.

To further probe the effect of interaction on the tunneling dynamics between the two wells of an asymmetric double well, we next increase Λ , keeping the asymmetry $C = 0.01$ fixed. The mean-field results of $p_L(t)$ and $p_R(t)$ for different Λ are shown in Fig. 2(c) and (d), respectively. We find a complementary effect of Λ on $p_L(t)$ and $p_R(t)$ at the mean-field level. While both $p_L(t)$ and $p_R(t)$ still oscillates back and forth, their amplitudes and frequencies vary with Λ in an opposite fashion. While stronger Λ facilitates oscillations of $p_L(t)$, it suppresses the oscillations of $p_R(t)$. Also, the frequencies of oscillations are found to decrease with increasing Λ for starting the dynamics from the left well, whereas when started from the right well, the frequencies increase with increasing Λ .

Qualitatively, the repulsive interaction pushes up the energy of the BEC with respect to the barrier height. For a sufficiently high barrier, the energy levels of the ground state and the first excited state of an asymmetric double well approximately coincide with the ground states of the left (lower) and the right (upper) wells, respectively. Therefore, when the initial state is prepared in the right (upper) well, the energy of the initial condensate becomes closer to the energy level of the first excited state of the asymmetric double well with increasing repulsive interaction Λ . Thus, the system tends more to remain in that state and the tunneling is more and more suppressed with increasing Λ . On the other hand, when the initial condensate is prepared in the left (lower) well, its energy is pushed away from the ground state of the asymmetric double well by the repulsive interaction and therefore, it becomes more prone to tunneling with increasing Λ .

At stronger Λ keeping N fixed, a mean-field theory may not be sufficient to describe the

system. Accordingly, we again refer to the symmetric double well case. Fig. 3(a) exhibits the time evolution of $p(t)$ for a symmetric double well calculated by MCTDHB with $M = 2$ orbitals. In the inset, the corresponding mean-field result of $p(t)$ is provided for comparison. We clearly see that, contrary to the mean-field result, the many-body result for $p(t)$ exhibits a collapse of the oscillations, thereby making a many-body calculation necessary for $\Lambda \geq 0.1$ for a system of $N = 1000$ bosons. Therefore, next, we calculate the $p_L(t)$ and $p_R(t)$ by MCTDHB method with $M = 2$ orbitals for the same parameters as in Fig. 2(c) and (d) for $N = 1000$ bosons. As an example, here we present the many-body results only for $\Lambda = 0.1$ in Fig. 3(b). The collapse of oscillations for both $p_L(t)$ and $p_R(t)$ can be seen on top of the overall mean-field effects described above. However, the collapse time differs: While the collapse for $p_L(t)$ is quicker compared to the symmetric double well, it is delayed for $p_R(t)$. We further found that, with an increase in Λ , the collapse is quicker for both the $p_L(t)$ and $p_R(t)$ for a fixed asymmetry C . On the other hand, for a fixed Λ , the collapse of both $p_L(t)$ and $p_R(t)$ is deferred with increasing C in terms of the number of Rabi cycles (recall that t_{Rabi} depends on C).

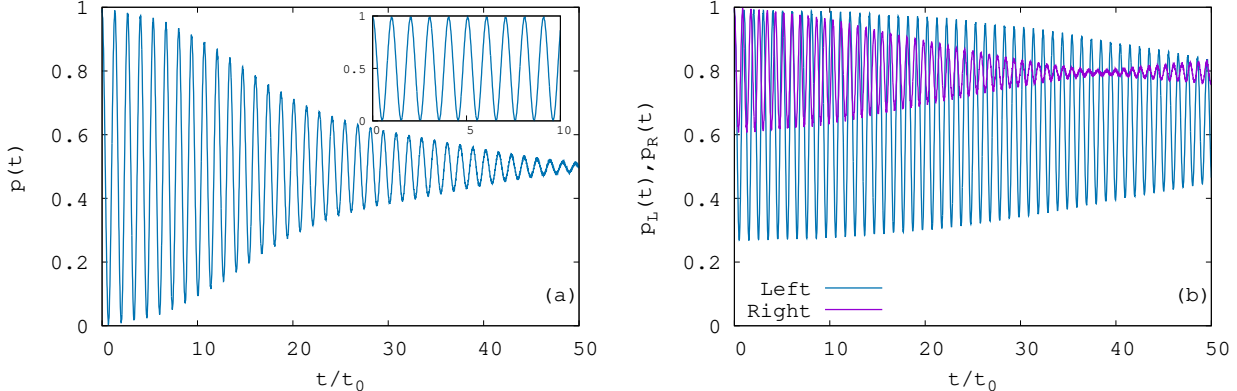


FIG. 3. (a) MCTDHB result of the time evolution of the survival probability $p(t)$ in the left well of a symmetric double well computed with $M = 2$ orbitals for a system of $N = 1000$ bosons and $\Lambda = 0.1$. The corresponding mean-field result is shown in the inset for comparison. (b) Corresponding MCTDHB result of the time evolution of the survival probabilities in the left [$p_L(t)$] and right [$p_R(t)$] well of an asymmetric double well with asymmetry $C = 0.01$. We used $M = 2$ orbitals for the computations of both $p_L(t)$ and $p_R(t)$ which are shown as the blue and magenta curves, respectively, as explained in the figure itself. The quantities shown are dimensionless.

2. Depletion and fragmentation

Having seen that a many-body calculation exhibits new features already for the time evolution of the survival probabilities at stronger Λ , next we would like to examine the time development of the depletion and fragmentation f (depending on Λ) of the condensate which is a purely many-body quantity. We found the BEC to become very slightly depleted with time for weak interactions such as $\Lambda = 0.01$. In Fig. 4 the time development of the depletion f of a BEC made of $N = 1000$ bosons is shown for different asymmetries C . We observe that, for all values of C considered here, f is extremely small and therefore the system is practically condensed. Explicitly, $n_1 > 999.999$ for the times shown in Fig. 4. Thus for such interaction strengths, the density per particle of the system is accurately described by the mean-field theory. Even then, time development of f exhibits some interesting features. First, the depletion is found to be maximum for the symmetric double well ($C = 0$) and gradually decreases with increasing C . Further, we observe an interesting difference between the time development of f for the left and right wells. Whereas for very small C the respective time evolutions of f are essentially same, the difference starts to develop with C and, while for $C \leq 0.005$, the depletion for the left well is larger than that for the right well, the situation reverses for $C = 0.01$.

Next we consider a stronger interaction $\Lambda = 0.1$. In Fig. 5(a) and (b), we plot the natural occupations $\frac{n_i}{N}$ for a system of $N = 1000$ interacting bosons as a function of time for different asymmetries C . We also plot the corresponding results for the symmetric double well ($C = 0$) in both panels as a reference. The results presented here are obtained with $M = 2$ orbitals. For all cases, we observe that starting from $\frac{n_1}{N} \approx 1$, the occupation in the first orbital $\frac{n_1}{N}$ gradually decreases with time. Simultaneously, the occupation in the second orbital $\frac{n_2}{N}$ slowly increases with time starting from a negligibly small value. Thus, with time the condensate becomes fragmented with a fragmentation fraction $f = \frac{n_2}{N}$. Finally, as the density oscillations collapse [see Fig. 3(b)], f reaches a plateau at $f = f_{col}$. Moreover, we see small oscillations in f prior to attaining the plateau. Such oscillations are the signatures in f of the time-dependent density oscillations. As the density oscillations collapse by the time f reaches the plateau, the oscillations in f are also heavily damped and remain so at the plateau.

Comparing the results for different asymmetries C , we find that both the growth rate of

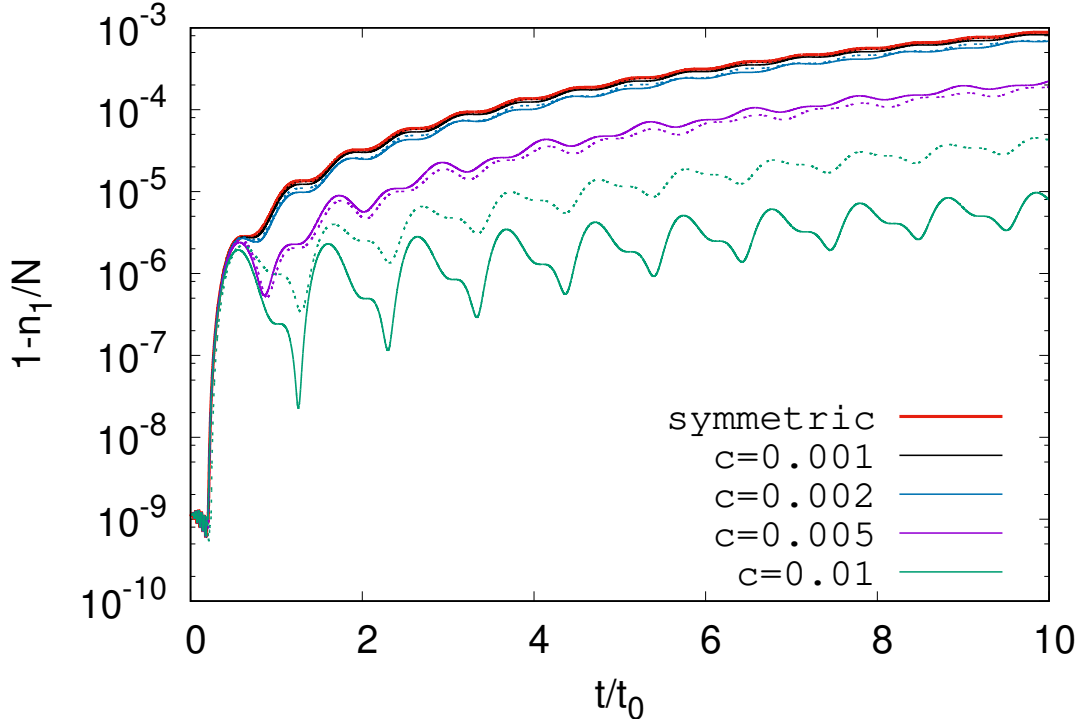


FIG. 4. The time development of the depletion per particle $f(= \sum_{j=2}^M \frac{n_j}{N} = 1 - \frac{n_1}{N})$ of the condensate of $N = 1000$ bosons in a symmetric double well (— curve), and an asymmetric double well trap with asymmetries $C = 0.001, 0.002, 0.005$ and 0.01 . Color codes are explained in the figure itself. While the solid line corresponds to f in the left well, the dotted line represents the same in the right well. The results shown here are computed by MCTDHB method with $M = 2$ orbitals. See text for further details. The quantities shown are dimensionless.

f and f_{col} depend on C . However, there is a crucial difference between the cases when the initial BEC state is prepared in the left [Fig. 5(a)] and the right wells [Fig. 5(b)]. For the left well, f_{col} first increases with increasing C and the condensate becomes more fragmented with reference to the symmetric double well until $C = 0.002$. With further increase in C , f_{col} decreases and the condensate becomes less fragmented. On the other hand, for the right well, f_{col} is found to decrease monotonically with increasing C , as far as $C \leq 0.005$.

We may understand these findings qualitatively by treating the small asymmetry as a perturbation. In [44] for each eigenstate $|E_n\rangle$ of the Bose-Hubbard dimer, its fragmentation f_n as a function of the eigenstate energy per particle E_n/N has been discussed. It has been

shown both analytically and numerically that f_n first increases with E_n/N , reaches a maximum of 50%, and then decreases with further increase of E_n/N . For a small perturbation, such qualitative functional dependence is expected to remain valid. Comparing the results in Fig. 5 with Fig. 3 of [44], we can infer that, for the parameters used in this work, the initial state for the symmetric double well lies on the upper part of the right-hand-branch of the f_n vs E_n/N curve (Fig. 3 of [44]). Now, the introduction of a small asymmetry C pulls down the energy for the left well and pushes up for the energy for the right well. Accordingly, f_{col} for the left well initially increases with C and then, with further increase of C and consequent decrease of the initial state energy, it crosses to the left branch of the f_n vs E_n/N curve (see Fig. 3 of [44]) and starts to decrease. On the other hand, with the increase in C the initial eigenstate energy for the right well monotonically increases resulting in a monotonic decrease of f_{col} (for not too large C). One would need to go beyond such a perturbation-based analysis to understand the behavior of fragmentation for $C > 0.005$ in the right well, see Fig. 5(b).

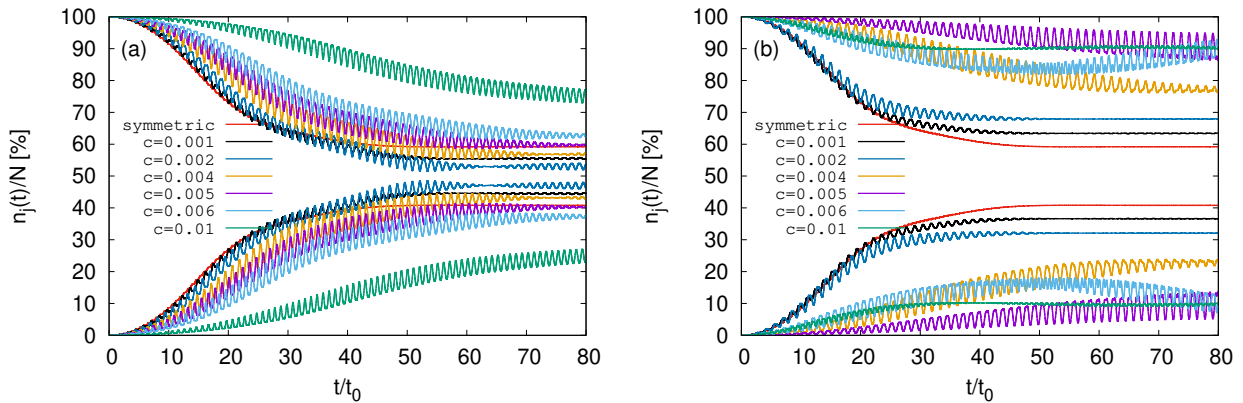


FIG. 5. Fragmentation per particle $f(= \frac{n_j}{M})$ of a system of $N = 1000$ bosons in an asymmetric double well with asymmetries $C = 0.001, 0.002, 0.004, 0.005, 0.006,$ and, 0.01 for interaction parameter $\Lambda = 0.1$ as a function of time t . Color codes are explained in each panel. Also the corresponding result for a symmetric double well is shown in each panel as a reference. The fragmentation per particle f of the system for preparing the initial condensate in the left well is shown in the panel (a) while the corresponding results for preparing the initial state in the right well is shown in panel (b). The results shown here are obtained with the MCTDHB method with $M = 2$ orbitals. The quantities shown are dimensionless.

3. Many-particle position and momentum variance

Next, we consider the time evolution of the many-particle position and momentum variances. These quantities characterize the fluctuations in the particles' positions and momenta in the junction. Although not easy to measure, they are fundamental quantum mechanical observables. Since these quantities depend on the actual number of depleted or fragmented atoms, it is expected that prominent signatures of the depletion and fragmentation of the condensate would show up in these variables. For $\Lambda = 0.01$, it has been shown above that the system remains practically condensed for a long time (see above) and therefore, its out-of-equilibrium dynamics should be adequately described by the mean-field theory. So, first we study the time evolution of the many-particle position variance $\frac{1}{N}\Delta_{\hat{X}}^2$ at the mean-field level. We present our results for different asymmetries C and a fixed $\Lambda = 0.01$ in Fig. 6(a) and (b) for preparing the initial BEC state in $V_L(x)$ and $V_R(x)$, respectively. For comparison, we also plot $\frac{1}{N}\Delta_{\hat{X}}^2$ for the symmetric double well in both panels.

We observe that for both $V_L(x)$ and $V_R(x)$ of the asymmetric double well trap, $\frac{1}{N}\Delta_{\hat{X}}^2$ oscillates with a frequency which equals to the Rabi frequency. This is in contrast to the case of the symmetric double well in which $\frac{1}{N}\Delta_{\hat{X}}^2$ oscillates with a frequency equal to twice the Rabi frequency. This is due to the incomplete tunneling between the two wells of the asymmetric double well trap, and that there is always a remnant in the each well which is further manifested in the irregular peaks of oscillations of $\frac{1}{N}\Delta_{\hat{X}}^2$. We observe that with increase in C starting from the symmetric double well ($C = 0$), the peaks of the oscillations of $\frac{1}{N}\Delta_{\hat{X}}^2$ first split into two sub-peaks which gradually turn into broad peaks for $C = 0.01$. Further, we observe high-frequency small-amplitude oscillations on top of the peaks of the large-amplitude oscillations. Such high-frequency oscillations are because of the breathing-mode oscillations of the system in the asymmetric double well and can be seen more vividly in the many-particle momentum variance (see below). Also, the minima of the oscillations are slightly higher than 0.5 for all times $t > 0$. Moreover, comparing the panels (a) and (b), we see that the peak values of the oscillations are slightly higher for the right well $V_R(x)$. All of these quantify the fluctuations in the particles' positions in the asymmetric double well at the mean-field level.

As discussed in Sec. III A, the many-particle position variance can deviate from their corresponding mean-field results even when the mean-field theory is expected to accurately

describe the density per particle of the system. So, we now study the time evolution of the many-particle position variance $\frac{1}{N}\Delta_X^2$ at the many-body level. For all cases, $\frac{1}{N}\Delta_X^2$ is found to grow in an oscillatory manner. For the symmetric double well ($C = 0$), the maxima of $\frac{1}{N}\Delta_X^2$ grow approximately quadratically, also see [47]. This growth is slower for an asymmetric double well, where the growth rate decreases with increasing C . This is consistent with our earlier observation that the depletion of the condensate is maximal in a symmetric double well. As observed at the mean-field level, here also, the oscillations of $\frac{1}{N}\Delta_X^2$ are irregular in nature. However, now the two sub-peaks are of unequal heights and the difference between them grows with time t for both $V_L(x)$ and $V_R(x)$. Comparison between the left [panel (c)] and the right wells [panel (d)] shows that, while the higher sub-peaks is on the left side for $V_L(x)$, it appears on the right side for $V_R(x)$. Further, while for $C = 0.005$ the maximal values for the $\frac{1}{N}\Delta_X^2$ in left well are larger than those in the right well, the situation reverses for $C = 0.01$. This is again consistent with our earlier observation (in Fig. 4) that the system in the left well is more depleted until $C = 0.005$, whereas the system in the right well is more depleted for $C = 0.01$.

Next, in Fig. 7, we plot the many-particle momentum variance $\frac{1}{N}\Delta_P^2$ of the system for starting the dynamics from $V_L(x)$ and $V_R(x)$, respectively. We studied $\frac{1}{N}\Delta_P^2$ both at the mean-field and the many-body levels. In Fig. 7(a) and (b) we present the mean-field results of $\frac{1}{N}\Delta_P^2$ for the left and the right wells, respectively. In each panel, we also plot $\frac{1}{N}\Delta_P^2$ for the symmetric double well for comparison. For all cases, we observe two oscillations associated with the time evolution of $\frac{1}{N}\Delta_P^2$: The first, with a larger amplitude and frequency equal to twice the Rabi frequency and, the second, with a smaller amplitude but a higher frequency. The first one is a manifestation of the density oscillations, whereas the second one is due to the breathing oscillations of the system. However, while in the symmetric double well the amplitude of the breathing mode oscillations are larger than those of the density oscillations, the situation is reversed in the asymmetric double well.

A closer examination of the high frequency breathing mode oscillations suggests that these may arise due to the transition of two bosons from the lowest energy band to the second band or one boson from the lowest band to the third band. An analysis by a linear-response theory in the line of Ref. [68] is required to attribute such high-frequency oscillations to a particular transitions unambiguously and accurately. In any case, it can be safely said that one needs to consider higher bands to take into account such high-frequency breathing

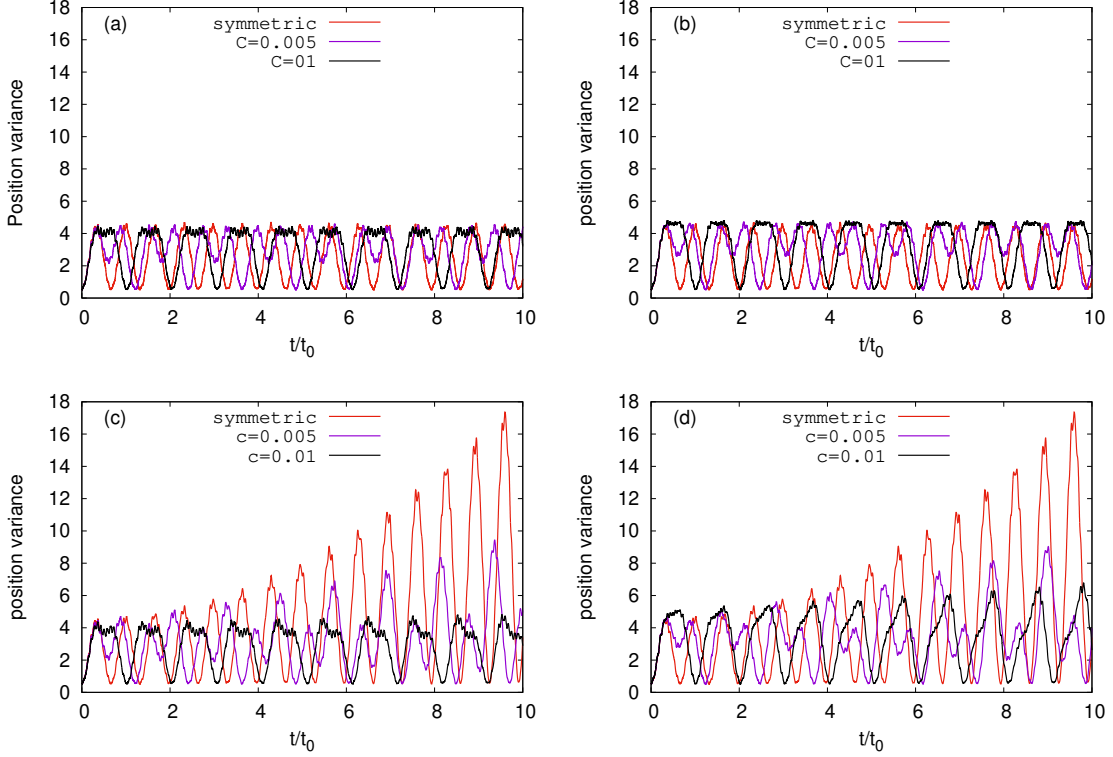


FIG. 6. many-particle position variance per particle $\frac{1}{N}\Delta_X^2$ of a system of $N = 1000$ bosons in a symmetric ($C = 0$) and an asymmetric double well with asymmetries $C = 0.005$ and 0.01 for interaction parameter $\Lambda = 0.01$ as a function of time t . Mean-field $\frac{1}{N}\Delta_X^2$ of the system for preparing the initial condensate state in the left and the right wells are shown in panel (a) and (b), respectively. Corresponding MCTDHB results with $M = 2$ orbitals for $\frac{1}{N}\Delta_X^2$ for preparing the initial condensate state in the right well are exhibited in panel (b) and (d), respectively. Color codes are explained in each panel. The quantities shown are dimensionless.

mode oscillations and this, of course, is beyond the scope of the standard Bose-Hubbard model. Moreover, though $\frac{1}{N}\Delta_P^2$ starts from the same value for both the left and right well, there is a Π -phase difference between the oscillations for the left well and the right well. Explicitly, the momentum variance first decreases when starting from the lower (left) well, whereas it first increases when starting from the higher (right) well. This can be understood from an energetic point of view. The BEC tunneling from the lower to upper well initially loses kinetic energy (momentum) and gains kinetic energy when tunneling from the higher to lower well. The momentum variance behaves accordingly.

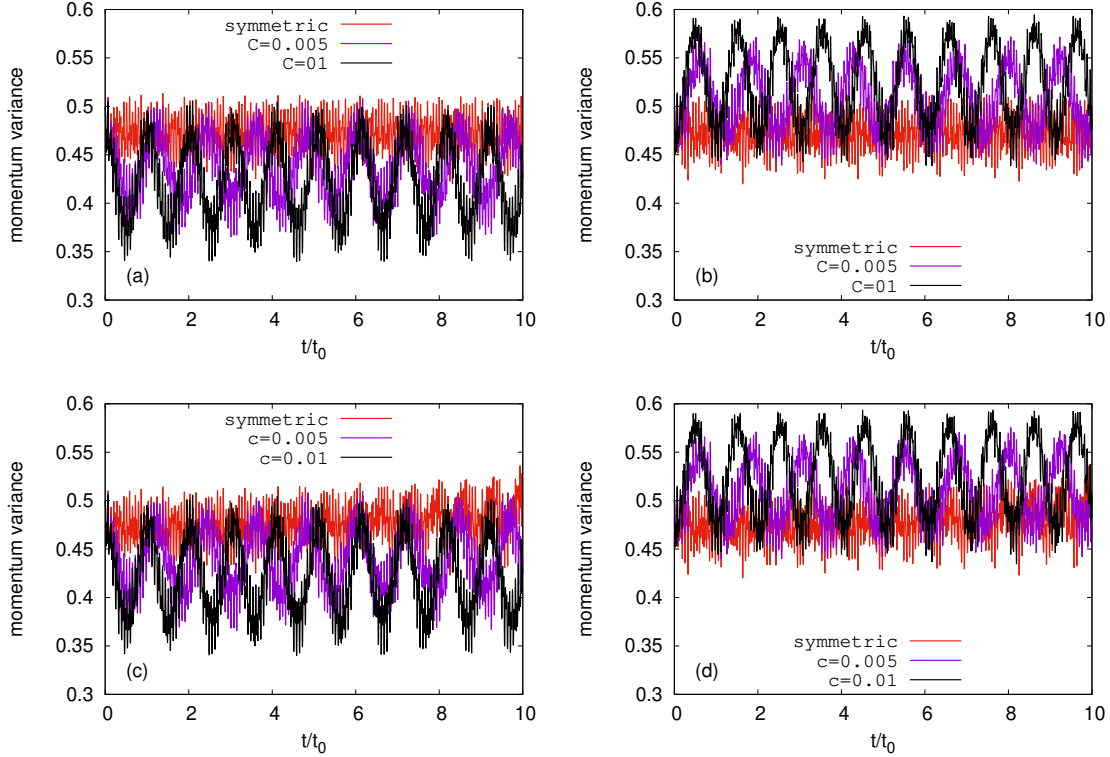


FIG. 7. many-particle momentum variance per particle $\frac{1}{N}\Delta_{\vec{p}}^2$ of a system of $N = 1000$ bosons in a symmetric ($C = 0$) and an asymmetric double well with asymmetries $C = 0.005$ and 0.01 for interaction parameter $\Lambda = 0.01$ as a function of time t . Mean-field $\frac{1}{N}\Delta_{\vec{p}}^2$ of the system for preparing the initial condensate state in the left and the right wells are shown in panel (a) and (b), respectively. Corresponding MCTDHB results with $M = 2$ orbitals for $\frac{1}{N}\Delta_{\vec{p}}^2$ for preparing the initial condensate state in the right well are exhibited in panel (b) and (d), respectively. Color codes are explained in each panel. The quantities shown are dimensionless.

Finally, we show the corresponding MCTDHB results of $\frac{1}{N}\Delta_{\vec{p}}^2$ with $M = 2$ orbitals in Fig. 7(c) and (d) for the left and the right wells, respectively. We find that the MCTDHB dynamics of $\frac{1}{N}\Delta_{\vec{p}}^2$ is similar to the corresponding mean-field dynamics. Actually, the many-particle momentum variance depends on the derivatives of the orbitals. For a weak asymmetry and a weakly interacting system, the shape of the orbitals deviate only slightly from their corresponding (non-interacting and) mean-field shape, and this leads to even smaller derivatives thereby producing practically same $\frac{1}{N}\Delta_{\vec{p}}^2$ both at the mean-field and the many-body levels.

B. Universality of the fragmentation dynamics in an asymmetric double well

A unique many-body feature predicted in the dynamics of BECs in a symmetric double well is the universality of the degree of fragmentation with respect to N for a fixed Λ [44]. It was first established by solving the many-body Schrödinger equation and then using the Bose-Hubbard dimer, it was also shown that the universality of fragmentation in a symmetric double well is a general many-body phenomenon [44]. Also, in the previous subsection, we have already found a significant effect of the asymmetry of the trap on the time evolution of the survival probabilities, fragmentation, and the many-particle position and momentum variances of BEC in an asymmetric double well trap. Naturally, questions arise if the universality of the fragmentation exists in an asymmetric trap and if so, how it is affected by the asymmetry of the trap.

Once again we start with the corresponding symmetric double well as a reference. In Fig. 8(a) we have plotted the natural occupations for different N keeping Λ fixed. As discussed above, we see that initially only one natural orbital is occupied with $\frac{n_1}{N} \approx 1$ and negligibly small f for all cases shown in Fig. 8. However, with time the second natural orbital starts to be occupied, the system becomes fragmented and, during the collapse of the density oscillations, the occupations of the natural orbitals reach the same plateau for different numbers of bosons N keeping Λ fixed. The values at the plateau are about $\frac{n_1}{N} = 60\%$ and $\frac{n_2}{N} = 40\%$, respectively. Hence for all cases, after the collapse of the density oscillations the system becomes $f_{col} \approx 40\%$ fragmented irrespective of N , showing a universal fragmentation dynamics [44].

Next, we consider an asymmetric double well with a very small asymmetry $C = 0.001$. Fig. 8(b) shows the results for $V_L(x)$ and Fig. 8(c) for $V_R(x)$. For both wells, qualitatively, we see the same dynamics as in the symmetric double well. We observe that following an oscillatory growth, f reaches the same plateau f_{col} irrespective of the number of particles N for a fixed Λ . Therefore, the universality of the fragmentation dynamics also persists in an asymmetric double well. However, quantitatively f_{col} for the left well differs from that for the right, $f_{col} \approx 45\%$ versus $f_{col} \approx 35\%$, respectively. Here, an interesting point is that f_{col} for the symmetric well is actually the mean of f_{col} for the two wells of the asymmetric double well. As shown in Ref [44], the fragmentation depends on the energy per particle. Since we have introduced the asymmetry by adding a linear slope of a fixed gradient, it pushes

up the right well by about the same amount as it pulls down the left well. Therefore, the changes in f_{col} for both wells are expected to be similar but in opposite directions, leading to the above relation between the fragmentation values.

As discussed earlier, the many-particle position variance $\frac{1}{N}\Delta_{\hat{X}}^2$ bears prominent signatures of the fragmentation. Hence, next, we study the time evolution of the many-particle position variance $\frac{1}{N}\Delta_{\hat{X}}^2$, both at the mean-field and the many-body levels, to explore the possible manifestation of the universality of the fragmentation dynamics. In Fig. 9 we plot the MCTDHB results with $M = 2$ orbitals of $\frac{1}{N}\Delta_{\hat{X}}^2$, for different N but the same Λ , as a function of time for starting the dynamics from both the left [panel (a)] and the right [panel (b)] wells. We also plot the corresponding mean-field results in both panels for comparison. In the mean-field theory, there is only one parameter Λ and therefore, we have only one curve for the time development of $\frac{1}{N}\Delta_{\hat{X}}^2$ for a particular Λ irrespective of N . On the other hand, at the many-body level, we find different time development for $\frac{1}{N}\Delta_{\hat{X}}^2$ for different N corresponding to the same Λ . For all N corresponding to the same Λ and both wells, $\frac{1}{N}\Delta_{\hat{X}}^2$ exhibits an oscillatory growth before reaching a saturation at a mean value $\frac{1}{N}\Delta_{\hat{X}}^2|_{sat}$. While the growth rate of $\frac{1}{N}\Delta_{\hat{X}}^2$ for different N corresponding to a fixed Λ are the same, the saturation values $\frac{1}{N}\Delta_{\hat{X}}^2|_{sat}$ increase with N . Moreover, we note that the time required to reach the saturation and the saturation values $\frac{1}{N}\Delta_{\hat{X}}^2|_{sat}$ are similar for both the left and right wells. Further, for both wells, the saturation value $\frac{1}{N}\Delta_{\hat{X}}^2|_{sat}^{N=N_1}$ for a BEC made of $N = N_1$ particles is of the same order of magnitude, viz., $\frac{1}{N}\Delta_{\hat{X}}^2|_{sat}^{N=N_1} \sim N_1$. For example, in Fig 9(a) and (b), for both wells, while $\frac{1}{N}\Delta_{\hat{X}}^2|_{sat}^{N=100} \sim 10^2$ for $N = 100$, it increases to $\frac{1}{N}\Delta_{\hat{X}}^2|_{sat}^{N=1000} \sim 10^3$ and $\frac{1}{N}\Delta_{\hat{X}}^2|_{sat}^{N=10000} \sim 10^4$ for $N = 1000$ and 10000, respectively.

These observations can be understood as follows. In Fig. 8, we have seen that f_{col} for the left well is only about 10% higher than that of the right well, for all N . Naturally, the actual occupation numbers n_2 are of the same order of magnitude for both wells for all N . Since $\frac{1}{N}\Delta_{\hat{X}}^2$ depends on the actual value of n_2 [67], its saturation values for a particular N are of the same order of magnitude (as a power of 10) for both the wells. Similarly, due to the universality of fragmentation dynamics, f_{col} corresponding to different N and same Λ have the same value for a particular well. Therefore, the actual number of fragmented atoms n_2 increases by a factor of $\frac{N_2}{N_1}$ for an increase of N from N_1 to N_2 . Accordingly, $\frac{1}{N}\Delta_{\hat{X}}^2|_{sat}$ also increases by a factor of $\frac{N_2}{N_1}$.

To stress this point further, in Fig. 9(c) and (d), we divide $\frac{1}{N}\Delta_{\hat{X}}^2|_{sat}$ by N , and plot

$\frac{1}{N^2}\Delta_{\hat{X}}^2$ for different N , keeping Λ fixed, for both wells. Again we find qualitatively similar time development of $\frac{1}{N^2}\Delta_{\hat{X}}^2$ for both wells. As before, for both wells, $\frac{1}{N^2}\Delta_{\hat{X}}^2$ also exhibit an oscillatory growth followed by an equilibration after the collapse of the density oscillations. However, the important point is that the curves for different N , keeping Λ same, saturate to the same mean value about which $\frac{1}{N^2}\Delta_{\hat{X}}^2$ keeps on oscillating. This is the signature of the universal fragmentation dynamics. Therefore, the universality of fragmentation is a quite robust many-body phenomena and its signature appears in all many-body quantities that depend on the occupation numbers of the natural orbitals.

IV. SUMMARY AND CONCLUDING REMARKS

Summarizing, we have examined how the BJJ dynamics is affected by the loss of symmetry of the confining double well potential for different interaction Λ . In an asymmetric double well, the two wells are no longer equivalent. Therefore, we have studied the dynamics by preparing the condensate initially in both the left and right wells. We have analyzed the dynamics by examining the time evolution of three physical quantities viz., the survival probability, depletion or fragmentation, and, the many-particle position and momentum variances.

We find that the impact of the asymmetry of the trap depends on the interaction Λ and the initial well. Overall, there is a suppression of tunneling between the two wells. However, the repulsive inter-atomic interaction facilitates the tunneling between the two wells when BEC is initially in the left well whereas the tunneling is further suppressed for starting the dynamics from the right well. For a sufficiently strong interaction Λ , the condensate becomes fragmented with time and the degree of fragmentation f depends on the asymmetry C and the initial well. The time evolution of the $\frac{1}{N}\Delta_{\hat{X}}^2$ bears prominent signature of the depletion of the system and deviates from its corresponding mean-field dynamics even for a weak Λ . In an asymmetric double well, both the frequencies and the amplitudes of the oscillations of $\frac{1}{N}\Delta_{\hat{X}}^2$ are found to be affected by the asymmetry. The dynamics of $\frac{1}{N}\Delta_{\hat{X}}^2$ in an asymmetric double well trap also bears signatures of the breathing-mode oscillations in addition to the density oscillations. However, the signatures of the breathing-mode oscillations are more prominent in the time evolution of the many-particle variance $\frac{1}{N}\Delta_{\hat{P}}^2$. While in the time evolution of $\frac{1}{N}\Delta_{\hat{P}}^2$, breathing-mode oscillations are more prominent than the density oscillations for the

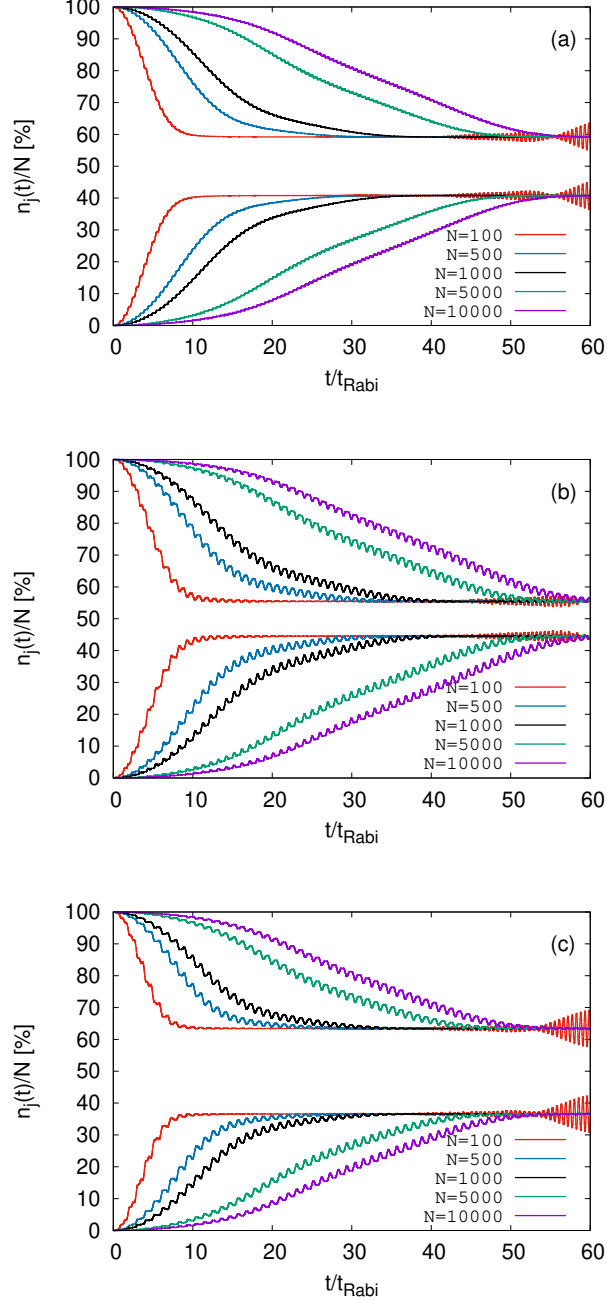


FIG. 8. Universality of the fragmentation dynamics for $\Lambda = 0.1$. (a) The natural occupations $\frac{n_j}{N}$ as a function of t for BECs consisting of different number N of bosons in the symmetric double well. For all N , we prepared the initial condensed state in the left well. (b) Same as in panel (a) but for an asymmetric double well of asymmetry $C = 0.001$. (c) The corresponding time evolution of $\frac{n_j}{N}$ for $C = 0.001$ when the initial condensate is prepared in the right well. In all panels, the upper curve represents $\frac{n_1}{N}$ while the lower curve shows the corresponding $\frac{n_2}{N}$. All the $\frac{n_j}{N}$ shown here are computed by the MCTDHB method with $M = 2$ orbitals. For further details, refer to the text. Color codes are explained in each panel. The quantities shown are dimensionless.

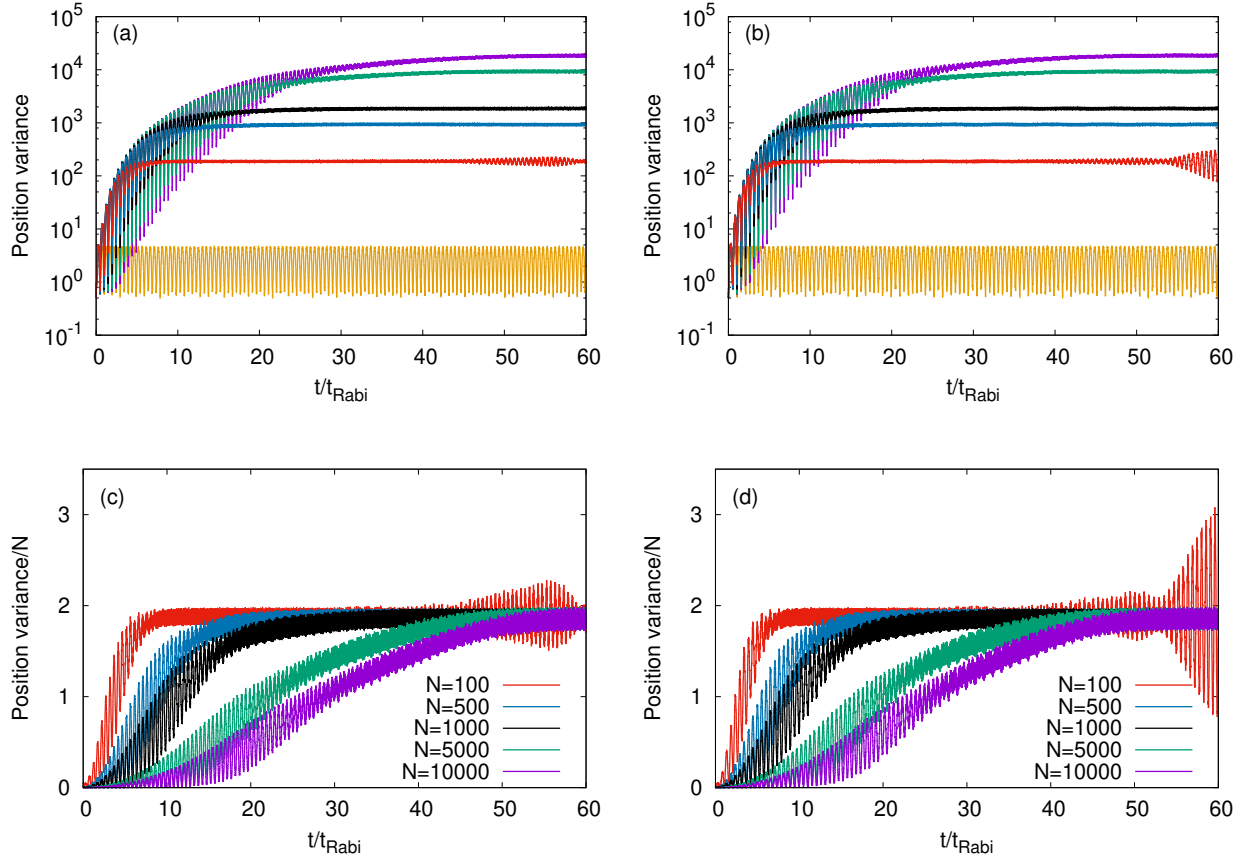


FIG. 9. Signature of universality of the fragmentation dynamics, as shown in Fig. 8, in the time evolution of the many-particle position variance. Time evolution of $\frac{1}{N} \Delta_{\hat{X}}^2$ (a) when the initial condensed state is prepared in the left well and (b) when the initial condensed state is prepared in the right well. In each panel, the yellow curve represents the mean-field result while the color code for the MCTDHB results are explained in panel (c) and (d). Corresponding time evolution of $\frac{1}{N^2} \Delta_{\hat{X}}^2$ (c) when the initial BEC is prepared in the left well and (d) when the initial BEC is prepared in the right well. Results are obtained by the MCTDHB method with $M = 2$ orbitals. For further details see the text. The quantities shown are dimensionless.

symmetric double well, both are distinctly visible in case of the asymmetric double well. Since breathing-mode oscillations arise from coupling to higher energy bands, such features are beyond the scope of the Bose-Hubbard dimer.

An important observation of our study is the universal fragmentation dynamics of asymmetric BJJ. However, the degree of universal fragmentation for BECs consisting of different N corresponding to the same Λ , depends on the initial well. Universality of fragmentation

is found to manifest in the same mean saturation value of the $\frac{1}{N^2}\Delta_X^2$ for different N corresponding to the same Λ at the many-body level. This means that the fluctuations of the positions of the particles in the junction show a universal behavior.

Macroscopic quantum tunneling is a fundamental quantum effect and is the underline mechanism for many physical events like Josephson junction. Also, BJJ is a paradigmatic device for understanding coherent quantum phenomena with potential applications in quantum interference technology, precision measurement, sensing, and, quantum metrology, etc. Particularly, in quantum interferometer, asymmetry of the trapping potential can be used as a means to shift the relative phase of the interferometer arms. Also, in view of a growing area of quantum science and technology, there is a strong need for accurate many-body characterization of BJJs which is able to take into account all dominant and participating degrees of freedom.

ACKNOWLEDGMENTS

This research was supported by the Israel Science Foundation (Grant No. 600/15). Computation time on the High Performance Computing system Hive of the Faculty of Natural Sciences at University of Haifa and on the Cray XC40 system Hazelhen at the High Performance Computing Center Stuttgart (HLRS) is gratefully acknowledged. SKH gratefully acknowledges the continuous hospitality at the Lewiner Institute for Theoretical Physics (LITP), Department of Physics, Technion - Israel Institute of Technology.

Appendix: Further details of the numerical computations and their convergence

Here we discuss the details of our numerical computations. We remind that the ansatz in MCTDHB theory is taken as the superposition of all possible permanents constructed by distributing N particles in M time-dependent orbitals which are then determined by a time-dependent variational principle. Further for $M = 1$, the ansatz Eq. (8) boils down to the mean-field ansatz, and using the time-dependent variational method with this ansatz gives the time-dependent Gross-Pitaevskii equation. Therefore, with our method, we can study the system at the mean-field level simply by considering $M = 1$ orbital. On the other hand, using a finite number M of orbitals, subject to the numerical convergence of

the quantities of interest, we can get a numerically accurate many-body description of the system. Here we point out that in the limit $M \rightarrow \infty$, the set of permanents $\{|\vec{n}; t\rangle\}$ spans the complete N -boson Hilbert space and thus the expansion Eq. (8) is exact, but in numerical calculations, computational limitations rule out that option. At the same, time-dependence of the permanents as well as the expansion coefficients allows one to consider a much shorter expansion than if only the expansion coefficients are taken to be time-dependent and thereby leads to a significant computational advantage.

In our numerical calculations, the many-body Hamiltonian is represented by 128 exponential discrete-variable-representation (DVR) grid points (using a Fast Fourier transformation routine) in a box size $[-10,10]$. We obtain the initial state for the time propagation, the many-body ground state of the BEC either in the left well or in the right well, by propagating the MCTDHB equations of motion [Eq. (9)] in imaginary time [46, 73]. For our numerical computations, we use the numerical implementation in [85, 86]. We keep on repeating the computation with increasing M until convergence is reached and thereby obtain the numerically accurate results.

Below we demonstrate the numerical convergence of the many-particle position and momentum variances. We already discussed in the text that the variance of any quantum operator is much more sensitive to the many-body effects compared to the oscillations in the survival probabilities and the fragmentation f . Actually, it is seen that the convergence of the momentum variance requires more numerical resources than the convergence of the position variance. Therefore, demonstration of convergence of the position and momentum variances will automatically imply the convergence of the survival probabilities and the fragmentation f with respect to M .

In an asymmetric double well, the two wells are not equivalent and therefore, in the text we discussed the dynamics of the system separately for preparing the initial BEC in the left well and in the right well. Accordingly here also, we discuss the convergence for both the cases separately, first when the initial BEC is prepared in the left well and then when the condensate is initially in the right well. We consider a system of $N = 10$ interacting bosons in an asymmetric double well with the asymmetry $C = 0.01$. Since in the limit $N \rightarrow \infty$, keeping Λ fixed, the many-body effects diminish and the density per particle of the system converge to its corresponding mean-field values [87–90], the convergence of the quantities for higher N values considered in the text (but same Λ values considered here) are actually

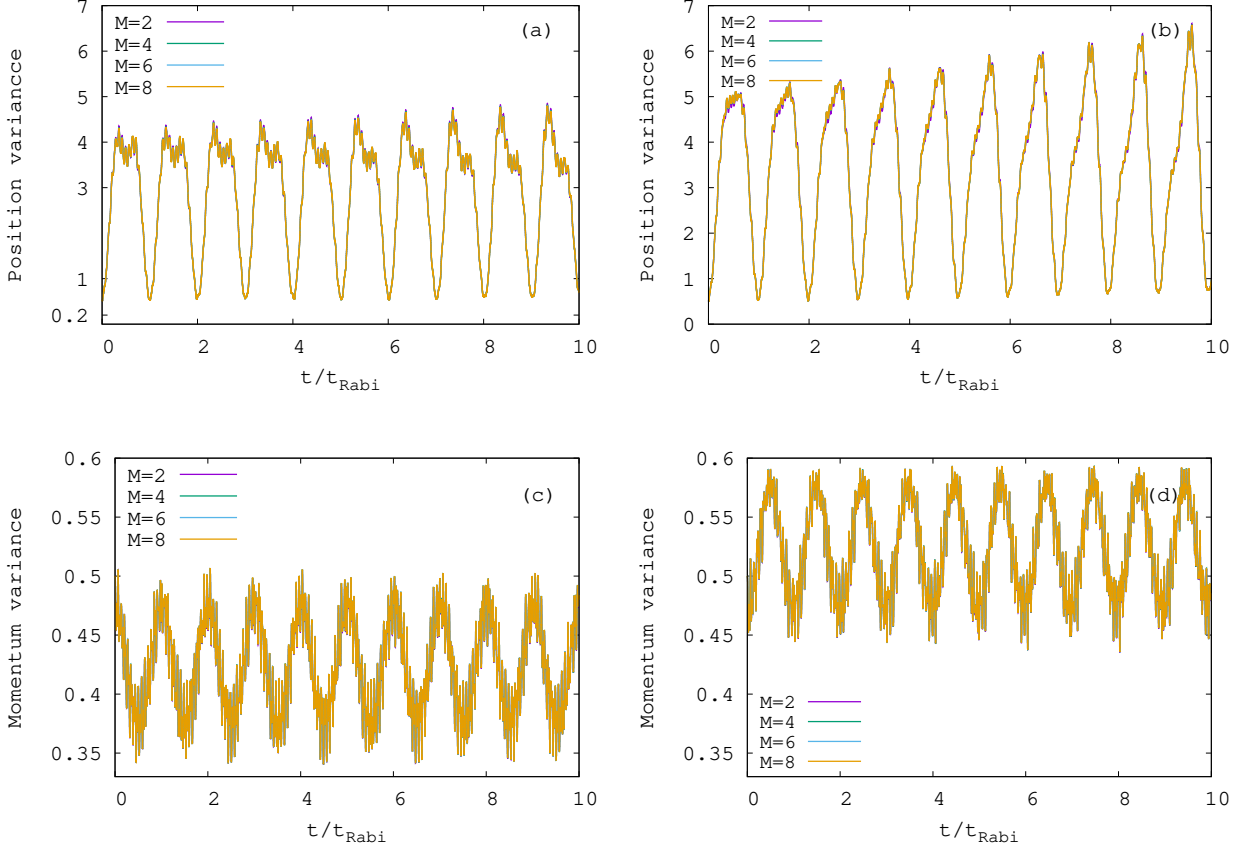


FIG. 10. Convergence of variances of the many-particle position and momentum operators with respect to the orbital number M for a system of $N = 10$ interacting bosons and $\Lambda = 0.01$ in the asymmetric double well trap of asymmetry $C = 0.01$. (a) Time-evolution of the many-particle position variance $\frac{1}{N}\Delta_X^2$ computed by MCTDHB method with different M when the initial condensate state is prepared in the left well. (b) The corresponding result for $\frac{1}{N}\Delta_X^2$ when the initial condensed state is prepared in the right well. (c) Time evolution of the momentum variance $\frac{1}{N}\Delta_P^2$ corresponding to (a). (d) Time evolution of the momentum variance $\frac{1}{N}\Delta_P^2$ corresponding to (b). For details see text. Color codes are explained in each panel. The quantities shown are dimensionless.

better than what is shown below.

We first consider $\Lambda = 0.01$. In Fig. 10 (a) and (b) we plot $\frac{1}{N}\Delta_X^2$ computed with $M = 2, 4, 6,$ and 8 for starting the dynamics from the left and right well, respectively. We see that, as discussed in the main text, $\frac{1}{N}\Delta_X^2$ exhibits a slow oscillatory growth for both wells. Furthermore, we see that there is an overall oscillation of $\frac{1}{N}\Delta_X^2$ in time with a frequency equal to twice the Rabi frequency. Also, on top of the peaks of these oscillations, there

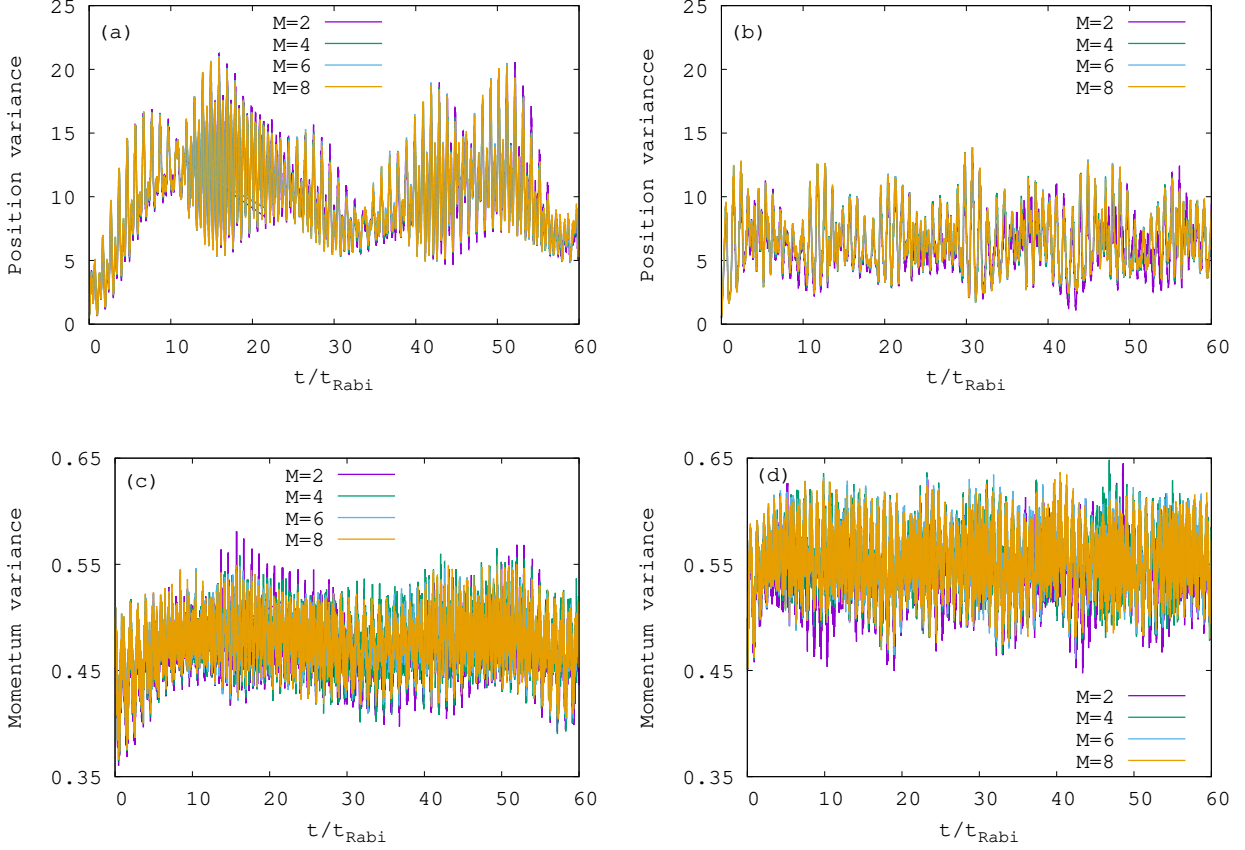


FIG. 11. Convergence of variances of many-particle position and momentum operators with respect to the orbital number M for a system of $N = 10$ interacting bosons and $\Lambda = 0.1$ in the asymmetric double well trap of asymmetry $C = 0.01$. (a) Time-evolution of the many-particle position variance $\frac{1}{N}\Delta_{\hat{X}}^2$ computed by MCTDHB method with different M when the initial condensate state is prepared in the left well. (b) The corresponding result for $\frac{1}{N}\Delta_{\hat{X}}^2$ when the initial condensed state is prepared in the right well. (c) Time evolution of momentum variance $\frac{1}{N}\Delta_{\hat{P}}^2$ corresponding to (a). (d) Time evolution of momentum variance $\frac{1}{N}\Delta_{\hat{P}}^2$ corresponding to (b). For details see text. Color codes are explained in each panel. The quantities shown are dimensionless.

is another oscillation with a higher frequency but smaller amplitude. The origin of these oscillations are discussed in the main text, see Sec. III A 3. Here, we observe that, for both cases, the results for $M = 2, 4, 6$, and 8 are in very good agreement with each other, such that not only the overall oscillations of $\frac{1}{N}\Delta_{\hat{X}}^2$ due to the density oscillations but also the small amplitude high-frequency oscillations on top of the peaks of the first ones are accurately described with $M = 2$.

To demonstrate the convergence of $\frac{1}{N}\Delta_P^2$, in Fig. 10(c) and (d), we plot the $\frac{1}{N}\Delta_P^2$ computed with $M = 2, 4, 6$, and 8 orbitals for preparing the condensate initially in the left and the right well, respectively. We clearly see that there are two oscillations associated with the time evolution of $\frac{1}{N}\Delta_P^2$ on top of one another, one with a larger amplitude and frequency equal to twice the Rabi frequency and the other one with a smaller amplitude but higher frequency. Once again, we see that the results of $\frac{1}{N}\Delta_P^2$ for different M practically overlap with each other, and the $M = 2$ is sufficient to describe both oscillations accurately.

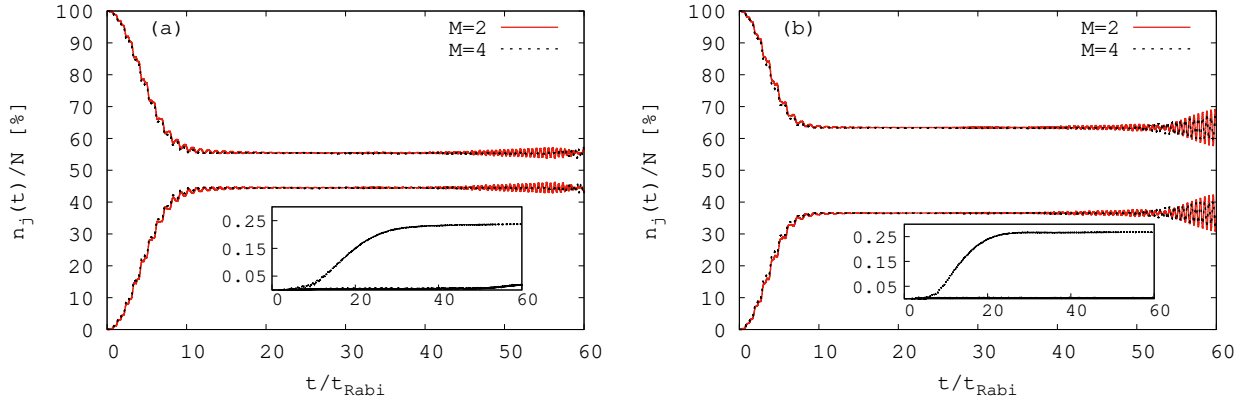


FIG. 12. Convergence of the universal fragmentation dynamics with respect to the orbital number M for a system of $N = 100$ interacting bosons and $\Lambda = 0.1$ in the asymmetric double well trap of asymmetry $C = 0.001$. (a) Initially the condensate is prepared in the left (lower) well. (b) The condensate prepared in the right (higher) well prior to the dynamics in the asymmetric double well. In each panel, the first two natural occupations viz., $\frac{n_1}{N}$ (upper curve) and $\frac{n_2}{N}$ (lower curve) are shown for computations with $M = 2$ and $M = 4$ orbitals in the MCTDHB method. Color codes are explained in each panel. In the insets of each panel, the higher natural occupations $\frac{n_3}{N}$ (upper curve) and $\frac{n_4}{N}$ (lower curve) computed by using $M = 4$ orbitals in the MCTDHB method are shown. See text for further details. The quantities shown are dimensionless.

Next, we consider the convergence for the stronger interaction $\Lambda = 0.1$. We plot $\frac{1}{N}\Delta_X^2$ computed with $M = 2, 4, 6$, and 8 time-adaptive orbitals for starting the dynamics from the left and right wells in Fig. 11 (a) and (b), respectively. As discussed in Sec. III A 3, there is an equilibration-like effect following which $\frac{1}{N}\Delta_X^2$ oscillates about a mean saturation value $\frac{1}{N}\Delta_X^2|_{sat}$. However, for $N = 10$ the system size is very small and this equilibration

is less pronounced. Clearly, the results of $\frac{1}{N}\Delta_{\hat{X}}^2$ obtained with $M = 2$ accurately describe all features of the time evolution of $\frac{1}{N}\Delta_{\hat{X}}^2$ while those for higher M practically overlap with each other. The corresponding results of $\frac{1}{N}\Delta_{\hat{P}}^2$ for starting the dynamics from the left and right wells, computed with $M = 2, 4, 6,$ and 8 orbitals, are shown in Fig. 11(c) and (d), respectively. We point out that in the main text, $\frac{1}{N}\Delta_{\hat{P}}^2$ is not computed for this interaction strength. For both cases, $\frac{1}{N}\Delta_{\hat{P}}^2$ keeps on oscillating about a mean value which depends on the well in which the condensate is initially prepared. Again, we see that the computations with $M = 2$ orbitals describe all the features of the time evolution of $\frac{1}{N}\Delta_{\hat{P}}^2$ and, as M increases, the curves corresponding to higher M starts to practically overlap with each other.

Finally, to explicitly show that the convergences of other quantities are also achieved with the same M as the variances, for the same system parameters, below as an example, we consider the convergence of the natural occupation numbers $\frac{n_j}{N}$. In Fig. 12 we plot $\frac{n_j}{N}$ for a system of $N = 100$ and $\Lambda = 0.1$ computed with $M = 2$ and 4 orbitals for preparing the initial condensate in the left [panel (a)] and right [panel (b)] wells of an asymmetric double well with $C = 0.001$. We found that the computation with $M = 4$ reproduces the same f as with $M = 2$ for both initial wells: The curves for the two largest occupation numbers $\frac{n_1}{N}$ and $\frac{n_2}{N}$ almost completely overlap with the corresponding results obtained with $M = 2$ and saturate about $\frac{n_1}{N} \approx 55\%$ and $\frac{n_2}{N} \approx 45\%$ for the left well and $\frac{n_1}{N} \approx 65\%$ and $\frac{n_1}{N} \approx 35\%$ for the right well, respectively. Also, the two smaller occupation numbers, viz. $\frac{n_3}{N}$ and $\frac{n_4}{N}$ obtained with $M = 4$ are negligibly small for both cases. While $\frac{n_3}{N}$ grows slowly with time only to saturate around 0.25% , $\frac{n_4}{N}$ shows very little increment from its initial near-zero value. Thus the convergences for quantities like $\frac{n_j}{N}$ are achieved with the same M as the variances for the same system parameters. Moreover, the near perfect agreement between the two results obtained with $M = 2$ and $M = 4$, respectively, along with the negligibly small values of $\frac{n_3}{N}$ and $\frac{n_4}{N}$ show that convergences improve with N keeping Λ fixed for a repulsive interaction. Finally and importantly, it also demonstrates that the universality of fragmentation is a robust many-body phenomenon and does not fissile out by using larger

numbers M of orbitals.

REFERENCES

- [1] M. H. Anderson, J. R. Ensher, M. R. Matthews, C. E. Wieman, and E. A. Cornell, Observation of Bose-Einstein condensation in a dilute atomic vapor, *Science* **269**, 198 (1995).
- [2] C. C. Bradley, C. A. Sackett, J. J. Tollett, and R. G. Hulet, Evidence of Bose-Einstein condensation in an atomic gas with attractive interactions, *Phys. Rev. Lett.* **75**, 1687 (1995).
- [3] K. B. Davis, M.-O. Mewes, M. R. Andrews, N. J. van Druten, D. S. Durfee, D. M. Kurn, and W. Ketterle, Bose-Einstein condensation in a gas of sodium atoms, *Phys. Rev. Lett.* **75**, 3969 (1995).
- [4] R. P. Feynman, Simulating physics with computers, *Int. J. Theoret. Phys.* **21**, 467 (1982).
- [5] M. Lewenstein, A. Sanpera, V. Ahufinger, B. Damski, A. Sen(De), and U. Sen, Ultracold atomic gases in optical lattices: mimicking condensed matter physics and beyond, *Adv. Phys.* **56**, 243 (2007).
- [6] M. Lewenstein, A. Sanpera, and V. Ahufinger, *Ultracold atoms in optical lattices: simulating quantum many-body systems*, (Oxford University Press, Oxford, 2012).
- [7] T. Sowiński, M. Brewczyk, M. Gajda, and K. Rzążewski, Dynamics and decoherence of two cold bosons in a one-dimensional harmonic trap, *Phys. Rev. A* **82** 053631 (2010).
- [8] A. Smerzi, S. Fantoni, S. Giovanazzi, and S. R. Shenoy, Quantum coherent atomic tunneling between two trapped Bose-Einstein condensates, *Phys. Rev. Lett.* **79**, 4950 (1997).
- [9] M. Albiez, R. Gati, J. Fölling, S. Hunsmann, M. Cristiani, and M. K. Oberthaler, Direct observation of tunneling and nonlinear self-trapping in a single bosonic Josephson junction, *Phys. Rev. Lett.* **95**, 010402 (2005).
- [10] G. J. Milburn, J. Corney, E. M. Wright, and D. F. Walls, Quantum dynamics of an atomic Bose-Einstein condensate in a double-well potential, *Phys. Rev. A* **55**, 4318 (1997).
- [11] J. Dobrzyniecki and T. Sowiński, Exact dynamics of two ultra-cold bosons confined in a one-dimensional double-well potential, *Eur. Phys. J. D* **70**, 83 (2016).
- [12] J. Hou, X. -W. Luo, K. Sun, T. Bersano, V. Gokhroo, S. Mossman, P. Engels, and C. Zhang, Momentum-Space Josephson Effects, *Phys. Rev. Lett.* **120**, 120401 (2018).

- [13] C. Menotti, J. R. Anglin, J. I. Cirac, and P. Zoller, Dynamic splitting of a Bose-Einstein condensate, *Phys. Rev. A* **63**, 023601 (2001).
- [14] F. Meier and W. Zwerger, Josephson tunneling between weakly interacting Bose-Einstein condensates, *Phys. Rev. A* **64** 033610 (2001).
- [15] A. N. Salgueiro, A.F.R. de Toledo Piza, G. B. Lemos, R. Drumond, M. C. Nemes, and M. Weidemüller, Quantum dynamics of bosons in a double-well potential: Josephson oscillations, self-trapping and ultralong tunneling times, *Eur. Phys. J. D* **44**, 537 (2007).
- [16] S. Zöllner, H.-D. Meyer, and P. Schmelcher, Few-boson dynamics in double wells: From single-atom to correlated pair tunneling, *Phys. Rev. Lett.* **100**, 040401 (2008).
- [17] L. D. Carr, D. R. Dounas-Frazer, and M. A. Garcia-March, Dynamical realization of macroscopic superposition states of cold bosons in a tilted double well, *Eur. Phys. Lett.* **90**, 10005 (2010).
- [18] L. J. LeBlanc, A. B. Bardou, J. McKeever, M.H. T. Extavour, D. Jervis, and J. H. Thywissen, Dynamics of a tunable superfluid junction, *Phys. Rev. Lett.* **106**, 025302 (2011).
- [19] L. Simon and W. T. Strunz, Analytical results for Josephson dynamics of ultracold bosons, *Phys. Rev. A* **86**, 053625 (2012).
- [20] Q.-Y. He, M. D. Reid, B. Opanchuk, R. Polkinghorne, L. E. C. Rosales-Zárata, and P. D. Drummond, Quantum dynamics in ultracold atomic physics, *Front. Phys.* **7**, 16 (2012).
- [21] J. Gillet, M. A. Garcia-March, T. Busch, and F. Sols, Tunneling, self-trapping, and manipulation of higher modes of a Bose-Einstein condensate in a double well *Phys. Rev. A* **89**, 023614 (2014).
- [22] Y. Liu and Y. Zhang, Two atoms in a double well: Exact solution with a Bethe ansatz, *Phys. Rev. A* **91**, 053610 (2015).
- [23] M. Tylutki, G. E. Astrakharchik, and A. Recati, Coherent oscillations in small Fermi-polaron systems, *Phys. Rev. A* **96**, 063603 (2017).
- [24] J. Dobrzyniecki, Xikun Li, Anne E. B. Nielsen, and Tomasz Sowiński, Effective three-body interactions for bosons in a double-well confinement, *Phys. Rev. A* **97**, 013609 (2018).
- [25] J. Dobrzyniecki and T. Sowiński, Effective two-mode description of a few ultra-cold bosons in a double-well potential, *Phys. Lett. A* **382**, 394 (2018).
- [26] R. Gati and M. K. Oberthaler, A bosonic Josephson junction, *J. Phys. B* **40**, R61 (2007).
- [27] H. Veksler and S. Fishman, Semiclassical analysis of Bose-Hubbard dynamics, *New J. Phys.*

- 17**, 053030 (2015).
- [28] T. Venumadhav, M. Haque, and R. Moessner, Finite-rate quenches of site bias in the Bose-Hubbard dimer, *Phys. Rev. B* **81**, 054305 (2010).
- [29] S. Levy, E. Lahoud, I. Shomroni, and J. Steinhauer, The a.c. and d.c. Josephson effects in a Bose-Einstein condensate, *Nature (London)* **449**, 579 (2007).
- [30] S. Raghavan, A. Smerzi, S. Fantoni, and S. R. Shenoy, Coherent oscillations between two weakly coupled Bose-Einstein condensates: Josephson effects, π oscillations, and macroscopic quantum self-trapping, *Phys. Rev. A* **59**, 620 (1999).
- [31] E. A. Ostrovskaya, Y. S. Kivshar, M. Lisak, B. Hall, F. Cattani, and D. Anderson, Coupled-mode theory for Bose-Einstein condensates, *Phys. Rev. A* **61**, 031601(R) (2000).
- [32] Y. Zhou, H. Zhai, R. Lü, Z. Xu, and L. Chang, Quantum coherence of double-well Bose-Einstein condensates: An SU(2) coherent-state path-integral approach, *Phys. Rev. A* **67**, 043606 (2003).
- [33] C. Lee, Adiabatic Mach-Zehnder interferometry on a quantized Bose-Josephson junction, *Phys. Rev. Lett.* **97**, 150402 (2006).
- [34] D. Ananikian and T. Bergeman, Gross-Pitaevskii equation for Bose particles in a double-well potential: Two-mode models and beyond, *Phys. Rev. A* **73**, 013604 (2006).
- [35] G. Ferrini, A. Minguzzi, and F. W. J. Hekking, Number squeezing, quantum fluctuations, and oscillations in mesoscopic Bose Josephson junctions, *Phys. Rev. A* **78**, 023606 (2008).
- [36] V. S. Shchesnovich and M. Trippenbach, Fock-space WKB method for the boson Josephson model describing a Bose-Einstein condensate trapped in a double-well potential, *Phys. Rev. A* **78**, 023611 (2008).
- [37] X. Y. Jia, W. D. Li, and J. Q. Liang, Nonlinear correction to the boson Josephson-junction model, *Phys. Rev. A* **78**, 023613 (2008).
- [38] M. Trujillo-Martinez, A. Posazhennikova, and J. Kroha, Nonequilibrium Josephson oscillations in Bose-Einstein condensates without dissipation, *Phys. Rev. Lett.* **103**, 105302 (2009).
- [39] T. Zibold, E. Nicklas, C. Gross, and M. K. Oberthaler, Classical bifurcation at the transition from Rabi to Josephson dynamics, *Phys. Rev. Lett.* **105**, 204101 (2010).
- [40] G. Spagnolli, G. Semeghini, L. Masi, G. Ferioli, A. Trenkwalder, S. Coop, M. Landini, L. Pezzè, G. Modugno, M. Inguscio, A. Smerzi, and M. Fattori, Crossing over from attractive to repulsive interactions in a tunneling bosonic Josephson junction, *Phys. Rev. Lett.* **118**, 230403

- (2017).
- [41] A. Burchinati, C. Fort, and M. Modugno, Josephson plasma oscillations and the Gross-Pitaevskii equation: Bogoliubov approach versus two-mode model, *Phys. Rev. A* **95**, 023627 (2017).
 - [42] K. Sakmann, A. I. Streltsov, O. E. Alon, and L. S. Cederbaum, Exact quantum dynamics of a bosonic Josephson junction, *Phys. Rev. Lett.* **103**, 220601 (2009).
 - [43] K. Sakmann, A. I. Streltsov, O. E. Alon, and L. S. Cederbaum, Quantum dynamics of attractive versus repulsive bosonic Josephson junctions: Bose-Hubbard and full-Hamiltonian results, *Phys. Rev. A* **82**, 013620 (2010).
 - [44] K. Sakmann, A. I. Streltsov, O. E. Alon, and L. S. Cederbaum, Universality of fragmentation in the Schrödinger dynamics of bosonic Josephson junctions, *Phys. Rev. A* **89**, 023602 (2014).
 - [45] S. K. Haldar and O. E. Alon, Impact of the range of the interaction on the quantum dynamics of a bosonic Josephson junction, *Chem. Phys.* **509**, 72 (2018).
 - [46] A. I. Streltsov, O. E. Alon, and L. S. Cederbaum, General variational many-body theory with complete self-consistency for trapped bosonic systems, *Phys. Rev. A* **73**, 063626 (2006).
 - [47] S. Klaiman, A. I. Streltsov, and O. E. Alon, Uncertainty product of an out-of-equilibrium many-particle system, *Phys. Rev. A* **93**, 023605 (2016).
 - [48] B. V. Hall, S. Whitlock, R. Anderson, P. Hannaford, and A. I. Sidorov, Condensate splitting in an asymmetric double well for atom chip based sensors, *Phys. Rev. Lett.* **98**, 030402 (2007).
 - [49] B. Juliá-Díaz, J. Martorell, and A. Polls, Bose-Einstein condensates on slightly asymmetric double-well potentials, *Phys. Rev. A* **81**, 063625 (2010).
 - [50] S. Hunn, K. Zimmermann, M. Hiller, and A. Buchleitner, Tunneling decay of two interacting bosons in an asymmetric double-well potential: A spectral approach, *Phys. Rev. A* **87**, 043626 (2013).
 - [51] H. M. Cataldo and D. M. Jezek, Dynamics in asymmetric double well condensates, *Phys. Rev. A* **90**, 043610 (2014).
 - [52] D. W. S. Carvalho, A. Foerster, and M. A. Gusmão, Ground states of spin-1 bosons in asymmetric double wells, *Phys. Rev. A* **91**, 033608 (2015).
 - [53] M. Gavrilov and J. Bechhoefer, Erasure without work in an asymmetric double-well potential, *Phys. Rev. Lett.* **117**, 200601 (2016).
 - [54] S. J. Kim, H. Yu, S. T. Gang, D. Z. Anderson, and J. B. Kim, Controllable asymmetric double

- well and ring potential on an atom chip, *Phys. Rev. A* **93**, 033612 (2016).
- [55] S. Paul and E Tiesinga, Wannier functions using a discrete variable representation for optical lattices, *Phys. Rev. A* **94**, 033606 (2016).
- [56] J. G. Cosme, M. F. Andersen, and J. Brand, Interaction blockade for bosons in an asymmetric double well, *Phys. Rev. A* **96**, 013616 (2017).
- [57] F. Dalfovo, S. Giorgini, L. P. Pitaevskii, and S. Stringari, Theory of Bose-Einstein condensation in trapped gases, *Rev. Mod. Phys.* **71**, 463 (1999).
- [58] P.-O. Löwdin, Quantum theory of many-particle systems. I. Physical interpretations by means of density matrices, natural spin-orbitals, and convergence problems in the method of configurational interaction, *Phys. Rev.* **97**, 1474 (1955).
- [59] A. J. Coleman and V. I. Yukalov, *Reduced density matrices: Coulson's challenge*, Lectures Notes in Chemistry Vol. 72 (Springer, Berlin, 2000).
- [60] *Reduced-density-matrix mechanics: With application to many-electron atoms and molecules*, edited by D. A. Mazziotti, Advances in Chemical Physics Vol. 134 (Wiley, New York, 2007).
- [61] K. Sakmann, A. I. Streltsov, O. E. Alon, and L. S. Cederbaum, Reduced density matrices and coherence of trapped interacting bosons, *Phys. Rev. A* **78**, 023615 (2008).
- [62] O. Penrose and L. Onsager, Bose-Einstein condensation and liquid Helium, *Phys. Rev.* **104**, 576 (1956).
- [63] P. Nozières and D. Saint James, Particle vs. pair condensation in attractive Bose liquids, *J. Phys. (France)* **43**, 1133 (1982);
- [64] P. Nozières, in *Bose-Einstein Condensation*, edited by A. Griffin, D. W. Snoke and S. Stringari (Cambridge University Press, Cambridge, England, 1996), p. 15.
- [65] R. W. Spekkens and J. E. Sipe, Spatial fragmentation of a Bose-Einstein condensate in a double-well potential, *Phys. Rev. A* **59**, 3868 (1999).
- [66] E. J. Mueller, T.-L. Ho, M. Ueda, and G. Baym, Fragmentation of Bose-Einstein condensates, *Phys. Rev. A* **74**, 033612 (2006).
- [67] S. Klaiman and O. E. Alon, Variance as a sensitive probe of correlation, *Phys. Rev. A* **91**, 063613 (2015).
- [68] M. Theisen and A. I. Streltsov, Many-body excitations and deexcitations in trapped ultracold bosonic clouds, *Phys. Rev. A* **94**, 053622 (2016).
- [69] S. Klaiman, R. Beinke, L. S. Cederbaum, A. I. Streltsov, and O. E. Alon, Variance of an

- anisotropic Bose-Einstein condensate, *Chem. Phys.* **509**, 45 (2018).
- [70] M. D. Girardeau and E. M. Wright, Breakdown of time-dependent mean-field theory for a one-dimensional condensate of impenetrable Bosons, *Phys. Rev. Lett.* **84**, 5239 (2000).
- [71] A. I. Streltsov, O. E. Alon, and L. S. Cederbaum, Role of excited states in the splitting of a trapped interacting Bose-Einstein condensate by a time-dependent barrier, *Phys. Rev. Lett.* **99**, 030402 (2007).
- [72] O. E. Alon, A. I. Streltsov, and L. S. Cederbaum, Multiconfigurational time-dependent Hartree method for bosons: Many-body dynamics of bosonic systems, *Phys. Rev. A* **77**, 033613 (2008).
- [73] A. U. J. Lode, K. Sakmann, O. E. Alon, L. S. Cederbaum, and A. I. Streltsov, Numerically exact quantum dynamics of bosons with time-dependent interactions of harmonic type, *Phys. Rev. A* **86**, 063606 (2012).
- [74] E. Fasshauer and A. U. J. Lode, Multiconfigurational time-dependent Hartree method for fermions: Implementation, exactness, and few-fermion tunneling to open space, *Phys. Rev. A* **93**, 033635 (2016).
- [75] J. Grond, J. Schmiedmayer, and U. Hohenester, Optimizing number squeezing when splitting a mesoscopic condensate, *Phys. Rev. A* **79**, 021603(R) (2009).
- [76] J. Grond, T. Betz, U. Hohenester, N. J. Mauser, J. Schmiedmayer, and T. Schumm, The Shapiro effect in atomchip-based bosonic Josephson junctions, *New J. Phys.* **13**, 065026 (2011).
- [77] R. Beinke, S. Klaiman, L. S. Cederbaum, A. I. Streltsov, and O. E. Alon, Many-body tunneling dynamics of Bose-Einstein condensates and vortex states in two spatial dimensions, *Phys. Rev. A* **92**, 043627 (2015).
- [78] A. U. J. Lode, B. Chakrabarti, and V. K. B. Kota, Many-body entropies, correlations, and emergence of statistical relaxation in interaction quench dynamics of ultracold bosons, *Phys. Rev. A* **92**, 033622 (2015).
- [79] A. U. J. Lode and C. Bruder, Fock-space WKB method for the boson Josephson model describing a Bose-Einstein condensate trapped in a double-well potential *Phys. Rev. A* **94**, 013616 (2016).
- [80] A. U. J. Lode, Multiconfigurational time-dependent Hartree method for bosons with internal degrees of freedom: Theory and composite fragmentation of multicomponent Bose-Einstein condensates, *Phys. Rev. A* **93**, 063601 (2016).
- [81] A. U. J. Lode and C. Bruder, Fragmented Superradiance of a Bose-Einstein Condensate in an

- Optical Cavity, *Phys. Rev. Lett.* **118**, 013603 (2017)
- [82] R. Roy, A. Gammal, M. C. Tsatsos, B. Chatterjee, B. Chakrabarti, and A. U. J. Lode, Phases, many-body entropy measures and coherence of interacting bosons in optical lattices, *Phys. Rev. A* **97**, 043625 (2018).
- [83] P. Kramer and M. Saracento, *Geometry of the time-dependent variational principle* (Springer, Berlin, 1981).
- [84] H.-J. Kull and D. Pfirsch, Generalized variational principle for the time-dependent Hartree-Fock equations for a Slater determinant, *Phys. Rev. E* **61**, 5940 (2000).
- [85] A. I. Streltsov and O. I. Streltsova, MCTDHB-Lab, version 1.5, 2015, <http://www.mctdhblab.com>.
- [86] A. I. Streltsov, L. S. Cederbaum, O. E. Alon, K. Sakmann, A. U. J. Lode, J. Grond, O. I. Streltsova, S. Klaiman, and R. Beinke, The multiconfigurational time-dependent Hartree for bosons package, version 3.x, Heidelberg/Kassel (2006-present), <http://mctdhb.org>.
- [87] E. H. Lieb, R. Seiringer, and J. Yngvason, Bosons in a trap: A rigorous derivation of the Gross-Pitaevskii energy functional, *Phys. Rev. A* **61**, 043602 (2000).
- [88] E. H. Lieb and R. Seiringer, Proof of Bose-Einstein condensation for dilute trapped gases, *Phys. Rev. Lett.* **88**, 170409 (2002).
- [89] L. Erdős, B. Schlein, and H.-T. Yau, Rigorous derivation of the Gross-Pitaevskii equation, *Phys. Rev. Lett.* **98**, 040404 (2007).
- [90] L. Erdős, B. Schlein, and H.-T. Yau, Derivation of the cubic non-linear Schrödinger equation from quantum dynamics of many-body systems, *Invent. Math.* **167**, 515 (2007).